Optimal resolution methods for the Klein-Gordon-Dirac system in the nonrelativistic limit regime

Wenfan Yi · Xinran Ruan · Chunmei Su

Abstract We propose and compare numerically spatial/temporal resolution of various efficient numerical methods for solving the Klein-Gordon-Dirac system (KGD) in the nonrelativistic limit regime. The KGD system involves a small dimensionless parameter $0 < \varepsilon \ll 1$ in this limit regime and admits rapid oscillations in time as $\varepsilon \to 0^+$. By adopting the Fourier spectral discretization for spatial derivatives followed with the time-splitting or exponential wave integrators based on some efficient quadrature rules in phase field, we propose four different numerical discretizations for the KGD system. The discretizations are all fully explicit and valid in one, two and three dimensions. Extensive numerical results demonstrate that these discretizations provide optimal numerical resolutions for the KGD system, i.e., under the mesh strategies $\tau = O(\varepsilon^2)$ and $h = O(1)$ with time step τ and mesh size h in terms of ε, they all perform well with uniform spectral accuracy in space and second-order accuracy in time. In addition, the ε-scalability of the best method is improved as $\tau = O(\varepsilon)$, which is much superior than that of the finite difference methods. For applications, we profile the dynamics of the KGD system in 2D with a honeycomb lattice potential, which depend greatly on the singular perturbation ε and the weak/strong interaction.

Keywords Klein-Gordon-Dirac system · Nonrelativistic limit regime · High oscillation · Yukawa interaction · Optimal resolution · Time-splitting technique · Wave integrator

Mathematics Subject Classification (2000) 35Q55 · 65M70 · 81Q05

1 Introduction

In quantum electrodynamics, the Klein-Gordon-Dirac system (KGD) represents the time-evolution of fast (relativistic) electrons and positrons within external time-dependent electromagnetic fields which coupled

Wenfan Yi
Beijing Computational Science Research Center, No. 10 West Dongbeiwang Road, Haidian District, Beijing 100193, People's Republic of China
E-mail: wfyi@csrc.ac.cn

Xinran Ruan (Corresponding author)
Department of Mathematics, National University of Singapore, Singapore 119076, Singapore
E-mail: ruan@ljll.math.upmc.fr

Chunmei Su
Department of Mathematics, University of Innsbruck, Innsbruck 6020, Austria
E-mail: sucm13@163.com

with a meson field through the Yukawa interaction [14, 17, 20, 37]. The dimensionless KGD system in d-dimensions ($d = 1, 2, 3$) reads

$$
\begin{cases}
\varepsilon^2 \partial_{tt} \phi(t, \mathbf{x}) - \Delta \phi(t, \mathbf{x}) + \dfrac{1}{\varepsilon^2} \phi(t, \mathbf{x}) = g \Psi^*(t, \mathbf{x}) \beta \Psi(t, \mathbf{x}), \\[2mm]
i \partial_t \Psi(t, \mathbf{x}) + \left[\dfrac{i}{\varepsilon} \sum_{j=1}^{d} \alpha_j \partial_j - \dfrac{\omega}{\varepsilon^2} \beta - \omega \left(V(t, \mathbf{x}) I_4 - \sum_{j=1}^{d} A_j(t, \mathbf{x}) \alpha_j \right) \right] \Psi(t, \mathbf{x}) = g \phi(t, \mathbf{x}) \beta \Psi(t, \mathbf{x}),
\end{cases}
\tag{1.1}
$$

with the initial data given as

$$
\phi(0, \mathbf{x}) = \phi^0(\mathbf{x}), \quad \partial_t \phi(0, \mathbf{x}) = \frac{1}{\varepsilon^2} \gamma(\mathbf{x}), \quad \Psi(0, \mathbf{x}) = \Psi^0(\mathbf{x}) = (\psi_1^0(\mathbf{x}), \psi_2^0(\mathbf{x}), \psi_3^0(\mathbf{x}), \psi_4^0(\mathbf{x}))^T,
\tag{1.2}
$$

where the unknowns $\phi := \phi(t, \mathbf{x}) \in \mathbb{R}$ and $\Psi := \Psi(t, \mathbf{x}) \in \mathbb{C}^4$ ($t > 0$, $\mathbf{x} \in \mathbb{R}^d$) present the real-valued scalar meson field and the complex-valued Dirac vector 'spinorfield', respectively. $V := V(t, \mathbf{x})$ is the real-valued electrical potential, $A_j(t, \mathbf{x})(1 \leq j \leq d)$ are the real-valued magnetic potentials, $0 < g \in \mathbb{R}$ is the coupling constant, $0 < \omega \leq 1$ is the ratio between the mass of the electron and the mass of the meson, $0 < \varepsilon \leq 1$ is a dimensionless parameter inversely proportional to the speed of light and the functions $\phi^0(\mathbf{x})$, $\gamma(\mathbf{x}) \in \mathbb{R}$ and $\Psi^0(\mathbf{x}) \in \mathbb{C}^4$ are independent of ε. Here, $i = \sqrt{-1}$ is the imaginary unit, $\partial_j = \frac{\partial}{\partial x_j}$ ($1 \leq j \leq d$) are the spatial partial derivatives and $\Delta = \sum_{j=1}^{d} \partial_j^2$ is the Laplace operator in d-dimensions. In addition, $\Psi^* = \overline{\Psi}^T$ is the conjugate transpose of Ψ, α_j and β are 4×4 matrices given as

$$
\alpha_j = \begin{pmatrix} \mathbf{0} & \sigma_j \\ \sigma_j & \mathbf{0} \end{pmatrix}, \quad j = 1, 2, 3, \quad \beta = \begin{pmatrix} I_2 & \mathbf{0} \\ \mathbf{0} & -I_2 \end{pmatrix},
\tag{1.3}
$$

with I_n being $n \times n$ identity matrix for $n \in \mathbb{N}$ and σ_j ($j = 1, 2, 3$) being the Pauli matrices given as

$$
\sigma_1 = \begin{pmatrix} 0 & 1 \\ 1 & 0 \end{pmatrix}, \quad \sigma_2 = \begin{pmatrix} 0 & -i \\ i & 0 \end{pmatrix}, \quad \sigma_3 = \begin{pmatrix} 1 & 0 \\ 0 & -1 \end{pmatrix}.
\tag{1.4}
$$

The above KGD (1.1) plays a fundamental role in quantum electrodynamics with wide applications in Hawking radiation and also appears in the Yukawa models for describing the nuclear force between nucleons [14, 26, 30, 35, 37]. Theoretically, the KGD (1.1) has gained a surge of attentions in the literature [1, 15, 16, 18, 19, 23, 24, 34, 36] and references therein on the existence and multiplicity of global existence, steady state solutions and well-posedness of the Cauchy problem. When the electromagnetic potentials are time-independent, i.e. $V(t, \mathbf{x}) = V(x)$, $A_j(t, \mathbf{x}) = A_j(\mathbf{x})$ for $1 \leq j \leq d$, the KGD (1.1) is dispersive, time symmetric and conserves the total *energy* which is defined as

$$
\begin{aligned}
\mathcal{E}(t) :=& \frac{\varepsilon^2}{2} \int_{\mathbb{R}^d} |\partial_t \phi(t, \mathbf{x})|^2 d\mathbf{x} + \frac{1}{2} \int_{\mathbb{R}^d} |\nabla \phi(t, \mathbf{x})|^2 d\mathbf{x} + \frac{1}{2\varepsilon^2} \int_{\mathbb{R}^d} \phi^2(t, \mathbf{x}) d\mathbf{x} \\
&+ \int_{\mathbb{R}^d} \left[\frac{i}{\varepsilon} \Psi^*(t, \mathbf{x}) \sum_{j=1}^{d} \alpha_j \partial_j \Psi(t, \mathbf{x}) - \frac{\omega}{\varepsilon^2} \Psi^*(t, \mathbf{x}) \beta \Psi(t, \mathbf{x}) - g \phi(t, \mathbf{x}) \Psi^*(t, \mathbf{x}) \beta \Psi(t, \mathbf{x}) \right] d\mathbf{x} \\
&- \omega \int_{\mathbb{R}^d} V(\mathbf{x}) |\Psi(t, \mathbf{x})|^2 d\mathbf{x} + \omega \sum_{j=1}^{d} \int_{\mathbb{R}^d} A_j(\mathbf{x}) \Psi^*(t, \mathbf{x}) \alpha_j \Psi(t, \mathbf{x}) d\mathbf{x}, \quad t \geq 0.
\end{aligned}
\tag{1.5}
$$

In addition, in lower dimensions ($d = 1, 2$), two components Dirac vector fields are usually employed and well-known in the (nonlinear) Dirac equation/system cases [4, 6, 17, 40], and the KGD (1.1) can be reduced to

$$
\begin{cases}
\varepsilon^2 \partial_{tt} \phi(t, \mathbf{x}) - \Delta \phi(t, \mathbf{x}) + \dfrac{1}{\varepsilon^2} \phi(t, \mathbf{x}) = g \Psi^*(t, \mathbf{x}) \sigma_3 \Psi(t, \mathbf{x}), \\[2mm]
i \partial_t \Psi(t, \mathbf{x}) + \left[\dfrac{i}{\varepsilon} \sum_{j=1}^{d} \sigma_j \partial_j - \dfrac{\omega}{\varepsilon^2} \sigma_3 - \omega \left(V(t, \mathbf{x}) I_2 - \sum_{j=1}^{d} A_j(t, \mathbf{x}) \sigma_j \right) \right] \Psi(t, \mathbf{x}) = g \phi(t, \mathbf{x}) \sigma_3 \Psi(t, \mathbf{x}),
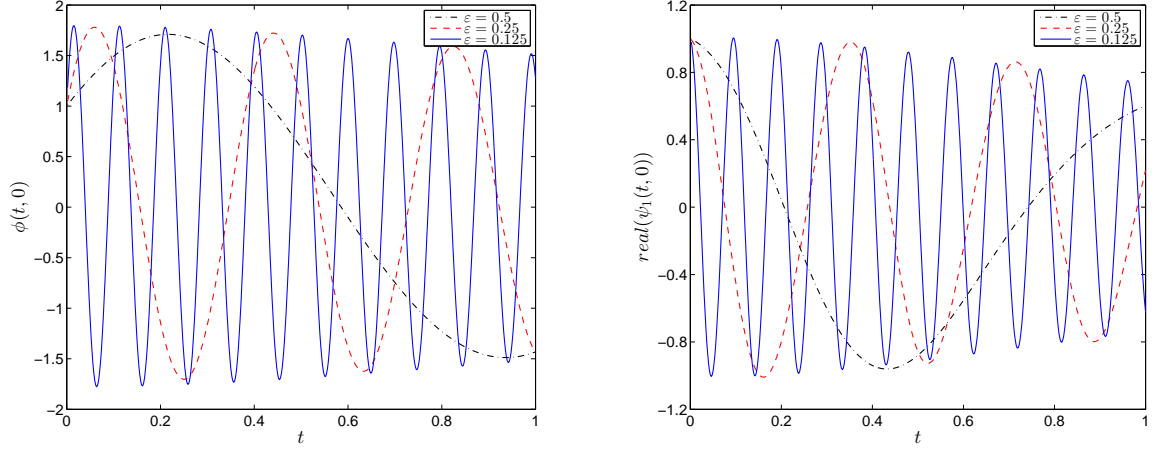\end{cases}
\tag{1.6}
$$

Fig. 1.1: The solutions $\phi(t, x = 0)$ (left) and $\psi_1(t, x = 0)$ (right) for different ε.

where $\phi \in \mathbb{R}$ and $\Psi \in \mathbb{C}^2$. This form is widely used in 1D and 2D, due to its simplicity.

For the numerical aspects of the KGD (1.1) (or (1.6)), the numerical approaches proposed in the literature are limited. In our recent work [17, 40], four conservative/non-conservative implicit/semi-implicit/explicit finite difference time domain methods (FDTD) have been analyzed for the KGD (1.1) (or (1.6)) with free electromagnetic potential. However, the Crank-Nicolson method (CNFD) is fully implicit and depends on a direct solver or an iterative solver which is quite time-consuming, while the other FDTD methods naturally suffer from stability problems with strong CFL-type constraints. Moreover, in the nonrelativistic limit regime, there exist highly oscillatory waves with wavelength at $O(\varepsilon^2)$ in time [17]. The temporal oscillatory structure of the solution $(\phi(t, \mathbf{x}), \Psi(t, \mathbf{x}))$ causes severe numerical burdens in practical computations. Even for the stable numerical discretizations (or under stability restrictions on meshing strategies), the approximations may come out completely wrong unless the temporal oscillation is fully resolved numerically. We have proved the discrete-H^1 error estimates of the FDTD methods in the nonrelativistic regime by employing the energy methods and cut-off technique [17], which suggest that the meshing strategy requirement (ε-scalability) of the FDTD methods should be

$$\tau = O(\varepsilon^3) \quad \text{and} \quad h = O(\sqrt{\varepsilon}).$$

They are under resolution and much time-consuming as $\varepsilon \to 0^+$. To illustrate the oscillatory structure further, Figure 1.1 shows the solutions in 1D for different ε, obtained numerically on a bounded interval $[-32, 32]$ with $\phi^0(x) = e^{-x^2/2}$, $\gamma(x) = \frac{3}{2} e^{-x^2/2}$, $\Psi^0(x) = (e^{-x^2/2}, e^{-(x-1)^2/2})^T$, $V(t, x) = (1-x)/(1+x^2)$, $A_1(t, x) = (x+1)^2/(1+x^2)$ and periodic boundary conditions ($real(f)$ denotes the real part of f).

Since the nonrelativistic limit behaviour of the KGD system is largely unknown, a discretization that performs well, which allows largest possible time step and mesh size for a given ε, is of great importance for the investigation and prediction of the dynamics and the wave interactions of the KGD (1.1) (or (1.6)). It is well known that the time-splitting Fourier pseudospectral method (TSFP) and wave integrator methods (including the Gautschi-type/Dauflhard-type exponential integrator Fourier pseudospectral method (GIFP/DIFP)) have many superior properties for integrating wave-type differential equations and are well illustrated and applied in [3, 9, 10, 25, 27–29, 31, 33, 39, 41] (and references therein). In [8], Bao et al. proposed a GIFP method for the (nonlinear) Klein-Gordon equation and verified that its ε-scalability is optimal with $\tau = O(1)$ and $\tau = O(\varepsilon^2)$ for the linear and nonlinear cases, respectively. Then Dong et al. numerically showed that the ε-scalability of the TSFP method for the nonlinear Klein-Gordon equation could be improved as $\tau = O(\varepsilon)$ and $h = O(1)$ [22]. They proved that the TSFP method is equivalent to the DIFP method for temporal approximations of the nonlinear Klein-Gordon equation by choosing the same starting values. While for the Dirac equation, in [5], Bao et al. compared and analysed several numerical methods

including the TSFP method and a symmetric exponential wave integrator Fourier pseudospectral method (sEWI-FP). Furthermore, they adopted another EWI-FP method for solving the nonlinear Dirac equation [6]. This method is asymmetric in time, but more stable than the sEWI-FP method. The results showed that the ε-scalability of the EWI-FP/sEWI-FP method is $\tau = O(\varepsilon^2)$ and $h = O(1)$ for the (nonlinear) Dirac equation. In addition, under suitable choices of the time step, the TSFP method whose ε-scalability is $\tau = O(\varepsilon)$ and $h = O(1)$, performs much better. For more recent progresses made on this topic, we refer to [4,7,11–13,32] and references therein. However, the nonlinear interaction terms bring new challenges for the implementations and mathematical analysis of the numerical methods. There is no clue to the performance of these two-types of approaches for the KGD (1.1) (or (1.6)), especially in highly oscillatory regime. The main purpose of this article is to investigate numerically the performance of these approaches with special attentions paid to how the convergence is affected by ε, and propose new numerical methods whose ε-scalability is optimal for both time and space in view of the inherent oscillatory nature for the KGD (1.1) (or (1.6)). The key ingredients of these approaches are: (i) applying the Fourier pseudospectral discretization for the spatial derivatives and, (ii) adopting a time-splitting technique or wave integrators based on some efficient quadrature rules for integrating the KGD (1.1) (or (1.6)) in the phase space.

This paper is organized as follows. In Section 2, we present the EWI-FP method for the KGD (1.6). Then, Section 3 is devoted to proposing the TSFP-type methods for the KGD (1.6). In Section 4, we show and compare the spatial/temporal resolution of four efficient discretizations for the KGD (1.6) within two special potential field cases, and profile the dynamics of the KGD system in 2D with a honeycomb lattice potential. Some concluding remarks are drawn in Section 5. Throughout this paper, we use $p \lesssim q$ to represent that there exists a generic constant C which is independent of τ, h and ε, such that $|p| \le Cq$.

2 Exponential wave integrator discretization

In this section, inspired by the ideas in [6,8,41], we propose an exponential wave integrator Fourier pseudospectral method (EWI-FP) for the KGD (1.6). The approach is based on the application of the Fourier pseudospectral discretization to the spatial derivatives followed by employing some wave integrators (such as the Gautschi-type/Dauflhard-type wave integrator) under appropriate chosen transmission conditions between different time intervals in the phase space. For simplicity of notations, we only illustrate the approaches in 1D. Generalizations to higher dimensions for the KGD (1.6) are straightforward for tensor grids and results remain valid without modification. In practical computation, due to the fast decay of the solution at the far field [17,40], we truncate the whole space problem onto a bounded interval Ω with periodic boundary conditions. The KGD (1.6) on $\Omega = (a,b)$ reads

$$\begin{cases} \varepsilon^2 \partial_{tt}\phi(t,x) - \partial_{xx}\phi(t,x) + \frac{1}{\varepsilon^2}\phi(t,x) = g\Psi^*(t,\mathbf{x})\sigma_3\Psi(t,x), & x \in \Omega, \quad t > 0, \\ i\partial_t\Psi(t,x) + \left[\frac{i}{\varepsilon}\sigma_1\partial_x - \frac{\omega}{\varepsilon^2}\sigma_3 - \omega(V(t,\mathbf{x})I_2 - A_1(t,\mathbf{x})\sigma_1)\right]\Psi(t,x) = g\phi(t,\mathbf{x})\sigma_3\Psi(t,x), \\ \phi(t,a) = \phi(t,b), \quad \partial_x\phi(t,a) = \partial_x\phi(t,b), \quad \Psi(t,a) = \Psi(t,b), \quad t \ge 0, \\ \phi(0,x) = \phi^0(x), \quad \partial_t\phi(0,x) = \frac{1}{\varepsilon^2}\gamma(x), \quad \Psi(0,x) = \Psi^0(x), \quad x \in \overline{\Omega}, \end{cases} \quad (2.1)$$

where $\phi := \phi(t,x) \in \mathbb{R}$ and $\Psi := \Psi(t,x) = (\psi_1(t,x),\psi_2(t,x))^T \in \mathbb{C}^2$.

Let's introduce some notations at the beginning. Choose the spatial mesh size $h = \frac{b-a}{M}$ and the temporal step size τ with M being an even positive integer, and the grid points and time steps are defined as

$$x_j := a + jh, \quad j \in \mathscr{T}_M^0 = \{j|j = 0,1,\cdots,M\}, \quad t_n := n\tau, \quad n = 0,1,2,\cdots. \quad (2.2)$$

Denote $X_M = \{U = (U_j)_{j \in \mathscr{T}_M^0}|U_j \in \mathbb{C}^2, U_0 = U_M\} \subset \mathbb{C}^{(M+1)\times 2}$, $\widetilde{X}_M = \{U = (U_j)_{j \in \mathscr{T}_M^0}|U_j \in \mathbb{R}, U_0 = U_M\} \subset \mathbb{R}^{M+1}$ and $[C_p(\overline{\Omega})]^2$ (or $C_p(\overline{\Omega})$) as the function space consisting of all periodic vector (or scalar) functions $U(x) : \overline{\Omega} \to \mathbb{C}^2$ (or $U(x) : \overline{\Omega} \to \mathbb{R}$). Let

$$Y_M = [Z_M]^2 \quad \text{and} \quad Z_M = \text{span}\{\varphi_l(x) = e^{i\mu_l(x-a)}, \quad l \in \mathscr{T}_M\}, \quad \mu_l = \frac{2l\pi}{b-a}, \quad (2.3)$$

where $\mathscr{T}_M = \{l | l = -M/2, -M/2 + 1, \cdots, M/2 - 1\}$. For any $U(x) \in [C_p(\overline{\Omega})]^2$ (or $U(x) \in C_p(\overline{\Omega})$) and $U \in X_M$ (or $U \in \widetilde{X}_M$), define $P_M : [L^2(\Omega)]^2 \to Y_M$ (or $L^2(\Omega) \to Z_M$) as the standard projection operator, $I_M : [C_p(\overline{\Omega})]^2 \to Y_M$ (or $C_p(\overline{\Omega}) \to Z_M$) and $I_M : X_M \to Y_M$ (or $\widetilde{X}_M \to Z_M$) as the standard interpolation operators, i.e.,

$$(P_M U)(x) = \sum_{l \in \mathscr{T}_M} \widehat{U}_l e^{i\mu_l(x-a)}, \quad (I_M U)(x) = \sum_{l \in \mathscr{T}_M} \widetilde{U}_l e^{i\mu_l(x-a)}, \quad x \in \overline{\Omega}, \tag{2.4}$$

with

$$\widehat{U}_l = \frac{1}{b-a} \int_a^b U(x) e^{-i\mu_l(x-a)} dx, \quad \widetilde{U}_l = \frac{1}{M} \sum_{j \in \mathscr{T}_{M-1}^0} U_j e^{-i\mu_l(x_j-a)}, \quad l \in \mathscr{T}_M, \tag{2.5}$$

where U_j is interpreted as $U(x_j)$ and we always use $U_{-1} = U_{M-1}$ and $U_{M+1} = U_1$ if they are involved.

The Fourier spectral discretization for the KGD (2.1) is to find $\phi_M := \phi_M(t,x) \in Z_M$ and $\Psi_M := \Psi_M(t,x) \in Y_M$, i.e.,

$$\phi_M(t,x) = \sum_{l \in \mathscr{T}_M} \widehat{(\phi_M)}_l(t) e^{i\mu_l(x-a)}, \quad \Psi_M(t,x) = \sum_{l \in \mathscr{T}_M} \widehat{(\Psi_M)}_l(t) e^{i\mu_l(x-a)}, \quad x \in \Omega, \quad t > 0, \tag{2.6}$$

such that

$$\varepsilon^2 \partial_{tt}\phi_M - \partial_{xx}\phi_M + \frac{1}{\varepsilon^2}\phi_M = P_M(g\Psi_M^* \sigma_3 \Psi_M), \tag{2.7}$$

$$i\partial_t \Psi_M + \frac{i}{\varepsilon}\sigma_1 \partial_x \Psi_M - \frac{\omega}{\varepsilon^2}\sigma_3 \Psi_M = P_M(g\phi_M \sigma_3 \Psi_M + \omega(V(t,x)I_2 - A_1(t,x)\sigma_1)\Psi_M), \tag{2.8}$$

with $\widehat{(\phi_M)}_l(t)$ and $\widehat{(\Psi_M)}_l(t)$ being the Fourier coefficients of the l-th mode. Plugging (2.6) into (2.7)-(2.8) and noticing the orthogonality of the Fourier functions, when t is near $t = t_n$ $(n \geq 0)$, we get

$$\frac{d^2}{ds^2}\widehat{(\phi_M)}_l(t_n+s) + \beta_l^2 \widehat{(\phi_M)}_l(t_n+s) = \frac{1}{\varepsilon^2}\widehat{(H_M^n)}_l(s), \quad l \in \mathscr{T}_M, \quad s > 0, \tag{2.9}$$

$$i\frac{d}{ds}\widehat{(\Psi_M)}_l(t_n+s) - \frac{1}{\varepsilon^2}\Gamma_l \widehat{(\Psi_M)}_l(t_n+s) = \widehat{(G_M^n)}_l(s), \quad l \in \mathscr{T}_M, \quad s > 0, \tag{2.10}$$

where

$$\widehat{(H_M^n)}_l(s) := \widehat{(H_M)}_l(t_n+s) = \widehat{(g\Psi_M^* \sigma_3 \Psi_M)}_l(t_n+s) = g\left((\widehat{|\psi_{1,M}|^2})_l - (\widehat{|\psi_{2,M}|^2})_l\right)(t_n+s),$$

$$\widehat{(G_M^n)}_l(s) := \widehat{(G_M)}_l(t_n+s) = \widehat{(g\phi_M \sigma_3 \Psi_M + \omega(VI_2 - A_1\sigma_1)\Psi_M)}_l(t_n+s),$$

and

$$\beta_l = \frac{1}{\varepsilon^2}\sqrt{\varepsilon^2\mu_l^2 + 1}, \quad \Gamma_l = \varepsilon\mu_l\sigma_1 + \omega\sigma_3 = \begin{pmatrix} \omega & \varepsilon\mu_l \\ \varepsilon\mu_l & -\omega \end{pmatrix} = Q_l D_l Q_l^*, \tag{2.11}$$

with

$$Q_l = \frac{1}{\sqrt{2\delta_l}}\begin{pmatrix} \sqrt{\delta_l + \omega} & -\sqrt{\delta_l - \omega} \\ \sqrt{\delta_l - \omega} & \sqrt{\delta_l + \omega} \end{pmatrix}, \quad D_l = \begin{pmatrix} \delta_l & 0 \\ 0 & -\delta_l \end{pmatrix}, \quad \delta_l = \sqrt{\omega^2 + \varepsilon^2\mu_l^2}. \tag{2.12}$$

Here, we proceed to apply the wave integrators for the ODEs (2.9)-(2.10) in time. Denoting $v_M(t_n+s,x) = \frac{\partial}{\partial s}\phi_M(t_n+s,x)$ and using the variation-of-constants formula, the general solutions of the ODEs (2.9)-(2.10) can be written as

$$\widehat{(\phi_M)}_l(t_n+s) = \widehat{(\phi_M)}_l(t_n)\cos(s\beta_l) + \widehat{(v_M)}_l(t_n)\frac{\sin(s\beta_l)}{\beta_l} + \frac{1}{\varepsilon^2\beta_l}\int_0^s \widehat{(H_M^n)}_l(t)\sin(\beta_l(s-t))dt, \tag{2.13}$$

$$\widehat{(v_M)}_l(t_n+s) = -\beta_l\widehat{(\phi_M)}_l(t_n)\sin(s\beta_l) + \widehat{(v_M)}_l(t_n)\cos(s\beta_l) + \frac{1}{\varepsilon^2}\int_0^s \widehat{(H_M^n)}_l(t)\cos(\beta_l(s-t))dt, \tag{2.14}$$

$$\widehat{(\Psi_M)}_l(t_n+s) = e^{-is\Gamma_l/\varepsilon^2}\widehat{(\Psi_M)}_l(t_n) - i\int_0^s e^{i(t-s)\Gamma_l/\varepsilon^2}\widehat{(G_M^n)}_l(t)dt, \quad l \in \mathscr{T}_M, \quad s > 0. \tag{2.15}$$

Considering the solutions (2.13)-(2.15) for $s \in [0, \tau]$ and requiring the solutions to be continuous at time t_n. Plugging $s = \tau$ into (2.13)-(2.15) implies

$$\widehat{(\phi_M)}_l(t_{n+1}) = \widehat{(\phi_M)}_l(t_n)\cos(\tau\beta_l) + \widehat{(v_M)}_l(t_n)\frac{\sin(\tau\beta_l)}{\beta_l} + \frac{1}{\varepsilon^2\beta_l}\int_0^\tau \widehat{(H_M^n)}_l(t)\sin(\beta_l(\tau - t))dt, \qquad (2.16)$$

$$\widehat{(v_M)}_l(t_{n+1}) = -\beta_l\widehat{(\phi_M)}_l(t_n)\sin(\tau\beta_l) + \widehat{(v_M)}_l(t_n)\cos(\tau\beta_l) + \frac{1}{\varepsilon^2}\int_0^\tau \widehat{(H_M^n)}_l(t)\cos(\beta_l(\tau - t))dt, \qquad (2.17)$$

$$\widehat{(\Psi_M)}_l(t_{n+1}) = e^{-i\tau\Gamma_l/\varepsilon^2}\widehat{(\Psi_M)}_l(t_n) - i\int_0^\tau e^{i(t-\tau)\Gamma_l/\varepsilon^2}\widehat{(G_M^n)}_l(t)dt, \quad l \in \mathscr{T}_M, \quad n \geq 0. \qquad (2.18)$$

Now the key problem is how to choose proper integral approximations in (2.16)-(2.18). In order to design an explicit scheme, we approximate the integrals in (2.16)-(2.17) by the Dauflhard-type quadrature rule, while the integral in (2.18) by the Gautschi-type quadrature rule given as

$$\int_0^\tau \widehat{(H_M^n)}_l(t)\sin(\beta_l(\tau - t))dt \approx \frac{\tau}{2}\widehat{(H_M^n)}_l(0)\sin(\tau\beta_l), \quad l \in \mathscr{T}_M, \quad n \geq 0, \qquad (2.19)$$

$$\int_0^\tau \widehat{(H_M^n)}_l(t)\cos(\beta_l(\tau - t))dt \approx \frac{\tau}{2}\left[\widehat{(H_M^{n+1})}_l(0) + \widehat{(H_M^n)}_l(0)\cos(\tau\beta_l)\right], \quad l \in \mathscr{T}_M, \quad n \geq 0, \qquad (2.20)$$

$$\int_0^\tau e^{i(t-\tau)\Gamma_l/\varepsilon^2}\widehat{(G_M^n)}_l(t)dt \approx \int_0^\tau e^{i(t-\tau)\Gamma_l/\varepsilon^2}\left[\widehat{(G_M^n)}_l(0) + \widehat{(G_M^n)}_l'(0)t\right]dt$$
$$= W_l^{(1)}(\tau)\widehat{(G_M^n)}_l(0) + W_l^{(2)}(\tau)\widehat{(G_M^n)}_l'(0), \quad l \in \mathscr{T}_M, \quad n \geq 0, \qquad (2.21)$$

where

$$W_l^{(1)}(\tau) = -i\varepsilon^2\Gamma_l^{-1}\left[I_2 - e^{-i\tau\Gamma_l/\varepsilon^2}\right], \quad W_l^{(2)}(\tau) = -i\varepsilon^2\tau\Gamma_l^{-1} + \varepsilon^4\Gamma_l^{-2}\left(I_2 - e^{-i\tau\Gamma_l/\varepsilon^2}\right),$$

and $\widehat{(G_M^n)}_l'(0) \approx \left(\widehat{(G_M^n)}_l(0) - \widehat{(G_M^{n-1})}_l(0)\right)/\tau$, when $n \geq 1$. $\widehat{(G_M^0)}_l'(0) = \widehat{(G_l^0)}'(0)$ can be deducted from the exact Dirac equation and the initial data in (2.1) as

$$\frac{\partial}{\partial t}G(0, x) = \partial_t W_2(0, x)\Psi^0(x) + W_2(0, x)\partial_t\Psi(0, x)$$
$$= \left(\frac{g}{\varepsilon^2}\gamma(x)\sigma_3 + \partial_t W_1(0, x)\right)\Psi^0(x) - W_2(0, x)\left[\frac{1}{\varepsilon}\sigma_1\partial_x + \frac{i\omega}{\varepsilon^2}\sigma_3 + iW_2(0, x)\right]\Psi^0(x),$$

with $W_1(t, x) = \omega(V(t, x)I_2 - A_1(t, x)\sigma_1)$ and $W_2(t, x) = g\phi(t, x)\sigma_3 + W_1(t, x)$.

In fact, we can observe that the practical computations of the KGD (2.1) are decoupled at each time step, i.e., one first updates the Dirac field $\Psi_M(t, x)$ by (2.18) with (2.21), and then updates the Klein-Gordon field $(\phi_M(t, x), v_M(t, x))$ by (2.16)-(2.17) with (2.19)-(2.20). In practice, due to the difficulties for computing the Fourier coefficients, here we refer to the Fourier pseudospectral discretization which replaces the projections by the interpolations. Let $(\phi_j^n, v_j^n, \Psi_j^n)$ be the approximation of $(\phi(t_n, x_j), v(t_n, x_j), \Psi(t_n, x_j))$ for $j \in \mathscr{T}_M^0$ and $n \geq 0$. Furthermore, denote $\Psi^n \in X_M$, $\phi^n \in \widetilde{X}_M$ and $v^n \in \widetilde{X}_M$ be the solution vectors at $t_n = n\tau$ with components Ψ_j^n, ϕ_j^n and v_j^n, respectively. Choosing $\Psi_j^0 = \Psi^0(x_j)$, $\phi_j^0 = \phi^0(x_j)$ and $v_j^0 = \varepsilon^{-2}\gamma^0(x_j)$, $j \in \mathscr{T}_M^0$, combining the Fourier pseudospectral discretization with the exponential wave integrators based on appropriate quadrature formulae, the EWI-FP reads

$$\Psi_j^{n+1} = \sum_{l \in \mathscr{T}_M}\widetilde{\Psi_l^{n+1}}e^{i\mu_l(x_j - a)}, \quad \phi_j^{n+1} = \sum_{l \in \mathscr{T}_M}\widetilde{\phi_l^{n+1}}e^{i\mu_l(x_j - a)}, \quad v_j^{n+1} = \sum_{l \in \mathscr{T}_M}\widetilde{v_l^{n+1}}e^{i\mu_l(x_j - a)}, \qquad (2.22)$$

where

$$\widetilde{\Psi_l^{n+1}} = Q_l e^{-i\tau D_l/\varepsilon^2}Q_l^*\widetilde{\Psi_l^n} - i\left[W_l^{(1)}(\tau)\widetilde{G_l^n} + W_l^{(2)}(\tau)\widetilde{(G_l^n)'}(0)\right], \quad l \in \mathscr{T}_M, \quad n \geq 0, \qquad (2.23)$$

$$\widetilde{\phi_l^{n+1}} = p_l^{(1)}\widetilde{\phi_l^n} + q_l^{(1)}\widetilde{v_l^n} + \kappa_l^{(1)}\widetilde{H_l^n}, \quad \widetilde{v_l^{n+1}} = p_l^{(2)}\widetilde{\phi_l^n} + q_l^{(2)}\widetilde{v_l^n} + \kappa_l^{(2)}\widetilde{H_l^n} + \xi_l^{(2)}\widetilde{H_l^{n+1}}, \quad l \in \mathscr{T}_M, \qquad (2.24)$$

with Γ_l, D_l, Q_l defined as in (2.12) and the coefficients given as

$$p_l^{(1)} = \cos(\tau\beta_l), \quad q_l^{(1)} = \frac{\sin(\tau\beta_l)}{\beta_l}, \quad \kappa_l^{(1)} = \frac{\tau}{2\varepsilon^2\beta_l}\sin(\tau\beta_l), \quad l \in \mathscr{T}_M, \tag{2.25}$$

$$p_l^{(2)} = -\beta_l\sin(\tau\beta_l), \quad q_l^{(2)} = \cos(\tau\beta_l), \quad \kappa_l^{(2)} = \frac{\tau}{2\varepsilon^2}\cos(\tau\beta_l), \quad \xi_l^{(2)} = \frac{\tau}{2\varepsilon^2}, \quad l \in \mathscr{T}_M. \tag{2.26}$$

The EWI-FP (2.22)-(2.24) is an explicit scheme. The memory cost is $O(M)$ and the computational load per time step is $O(M\ln M)$ thanks to the FFT. Similar to the Von Neumann analysis in [5,6,8], we also have the following lemma with the proof omitted for brevity.

Lemma 2.1 *The EWI-FP (2.22)-(2.24) is stable under the stability conditions*

$$0 < \tau \lesssim 1, \quad h > 0, \quad 0 < \varepsilon \leq 1. \tag{2.27}$$

Remark 2.1 As stated in [8], when $n \geq 1$, (2.16) can be reformulated into a three-level scheme as

$$\widehat{(\phi_M)}_l(t_{n+1}) = 2\widehat{(\phi_M)}_l(t_n)\cos(\tau\beta_l) - \widehat{(\phi_M)}_l(t_{n-1}) + \frac{1}{\varepsilon^2\beta_l}\int_0^\tau\left[\widehat{(H_M^n)}_l(t) + \widehat{(H_M^n)}_l(-t)\right]\sin(\beta_l(\tau - t))dt.$$

In this formalism, one can eliminate the time derivative $\upsilon(t, x)$ if it is not of interests. For benchmark comparisons, we recall the Gautschi-type exponential wave integrator Fourier pseudospectral method (GIFP) proposed in [8] for the Klein-Gordon component in the KGD (2.1). The three-level GIFP method reads: finding

$$\phi_j^{n+1} = \sum_{l \in \mathscr{T}_M}\widetilde{\phi_l^{n+1}}e^{i\mu_l(x_j-a)}, \quad j \in \mathscr{T}_M^0, \quad n \geq 0, \tag{2.28}$$

which satisfies

$$\widetilde{\phi}_l^1 = p_l^0\widetilde{\phi}_l^0 + q_l^0\widetilde{\gamma}_l + \kappa_l^0\widetilde{H}_l^0(0) + \xi_l^0(\widetilde{H_l^0})'(0), \quad \widetilde{\phi}_l^{n+1} = -\widetilde{\phi}_l^{n-1} + p_l^n\widetilde{\phi}_l^n + \kappa_l^n\widetilde{H}_l^n(0), \quad l \in \mathscr{T}_M, \quad n \geq 1, \tag{2.29}$$

with $(\widetilde{H_l^0})'(0)$ being deducted from the exact Dirac equation and the initial data as

$$\frac{\partial}{\partial t}H(0, x) = -\frac{g}{\varepsilon}[\partial_x(\Psi^0)^*(x)\sigma_1\sigma_3\Psi^0(x) + (\Psi^0)^*(x)\sigma_3\sigma_1\partial_x\Psi^0(x)], \tag{2.30}$$

and the coefficients given as

$$p_l^0 = \cos(\tau\beta_l), \quad q_l^0 = \frac{1}{\varepsilon^2\beta_l}\sin(\tau\beta_l), \quad \kappa_l^0 = \frac{1}{\varepsilon^2\beta_l^2}(1 - \cos(\tau\beta_l)), \quad \xi_l^0 = \frac{\tau}{\varepsilon^2\beta_l^2} - \frac{1}{\varepsilon^2\beta_l^3}\sin(\tau\beta_l), \tag{2.31}$$

$$p_l^n = 2\cos(\tau\beta_l), \quad \kappa_l^n = \frac{2}{\varepsilon^2\beta_l^2}(1 - \cos(\tau\beta_l)), \quad l \in \mathscr{T}_M, \quad n \geq 1. \tag{2.32}$$

The above GIFP method is also explicit and the computational cost is the same as the EWI-FP method. However, the finite time error estimate of the GIFP method given in [8] suffers a CFL-type stability condition $\tau \lesssim h$, that is also the reason why we choose the Dauflhard-type integrator for the Klein-Gordon component in the above derivation of (2.24) in the EWI-FP method.

3 Time-splitting integrator discretization

In this section, we revisit the time-splitting Fourier pseudospectral method (TSFP) in [2,5,6,22,33,38], and apply it for the KGD (1.6). This method is based on the application of the Fourier pseudospectral approximation to spatial derivatives followed by a time-splitting integrator in time discretization to an equivalent first-order system. We use the same notations as those in Section 2.

Introducing $\upsilon(t,x) = \partial_t\phi(t,x)$, then the KGD (2.1) is equivalent to the first-order-in-time system as

$$i\partial_t\Psi(t,x) + \left[\frac{i}{\varepsilon}\sigma_1\partial_x - \frac{\omega}{\varepsilon^2}\sigma_3 - \omega(V(t,x)I_2 - A_1(t,x)\sigma_1)\right]\Psi(t,x) = g\phi(t,\mathbf{x})\sigma_3\Psi(t,x), \tag{3.1}$$

$$\partial_t\phi(t,x) - \upsilon(t,x) = 0, \tag{3.2}$$

$$\varepsilon^2\partial_t\upsilon(t,x) - \partial_{xx}\phi(t,x) + \frac{1}{\varepsilon^2}\phi(t,x) = g\Psi^*(t,\mathbf{x})\sigma_3\Psi(t,x), \tag{3.3}$$

for $x \in \Omega$ and $t > 0$ with the initial data and boundary conditions given as

$$\phi(0,x) = \phi^0(x), \quad \upsilon(0,x) = \frac{1}{\varepsilon^2}\gamma(x), \quad \Psi(0,x) = \Psi^0(x), \quad x \in \overline{\Omega},$$

$$\phi(t,a) = \phi(t,b), \quad \partial_x\phi(t,a) = \partial_x\phi(t,b), \quad \upsilon(t,a) = \upsilon(t,b), \quad \Psi(t,a) = \Psi(t,b), \quad t \geq 0.$$

We proceed to adopt a time-splitting technique combined with the Fourier spectral discretization for the Dirac component (3.1) and the Klein-Gordon component (3.2)-(3.3) in the above first-order system, respectively, which is divided into solving four subproblems. The key point to an efficient implementation of the time-splitting technique for the Dirac component (3.1) is to solve two subproblems efficiently from time t_n to t_{n+1}, i.e., firstly solve

$$\partial_t\Psi(t,x) = -\frac{1}{\varepsilon}\sigma_1\partial_x\Psi(t,x) - \frac{i\omega}{\varepsilon^2}\sigma_3\Psi(t,x), \quad x \in \Omega, \quad t > 0, \tag{3.4}$$

with the periodic boundary conditions for time step of length τ, followed by solving

$$\partial_t\Psi(t,x) = -i[g\phi(t,x)\sigma_3 + \omega(V(t,x)I_2 - A_1(t,x)\sigma_1)]\Psi(t,x), \quad x \in \Omega, \quad t > 0, \tag{3.5}$$

for the same time step. Meanwhile, the implementation of the time-splitting technique for the Klein-Gordon component (3.2)-(3.3) is to solve another two subproblems from t_n to t_{n+1}, i.e., one firstly solves

$$\partial_t\phi(t,x) = 0, \quad x \in \Omega, \quad t > 0, \tag{3.6}$$

$$\partial_t\upsilon(t,x) = \frac{1}{\varepsilon^2}g\Psi^*(t,x)\sigma_3\Psi(t,x), \quad x \in \Omega, \quad t > 0, \tag{3.7}$$

with the periodic boundary conditions for time step of length τ, then solves

$$\partial_t\phi(t,x) - \upsilon(t,x) = 0, \quad x \in \Omega, \quad t > 0, \tag{3.8}$$

$$\partial_t\upsilon(t,x) = \frac{1}{\varepsilon^2}\partial_{xx}\phi(t,x) - \frac{1}{\varepsilon^4}\phi(t,x), \quad x \in \Omega, \quad t > 0, \tag{3.9}$$

for the same time step.

For the Dirac component, when $A_1(t,x) \equiv 0$, the ODEs (3.5) can be integrated analytically in time as

$$\Psi(t_{n+1},x) = e^{-i\int_{t_n}^{t_{n+1}} W(t,x)dt}\Psi(t_n,x), \quad x \in \Omega, \quad n \geq 0, \tag{3.10}$$

where $\int_{t_n}^{t_{n+1}} W(t,x)dt = \int_{t_n}^{t_{n+1}} g\phi(t,x)\sigma_3 + \omega V(t,x)I_2 dt = \phi^{(1)}(x)\sigma_3 + V^{(1)}(x)I_2 = P_1\Lambda(x)P_1^*$ with $\phi^{(1)}(x) = g\int_{t_n}^{t_{n+1}}\phi(t,x)dt$, $V^{(1)}(x) = \omega\int_{t_n}^{t_{n+1}}V(t,x)dt$, $\Lambda(x) = \text{diag}(\Lambda_+(\mathbf{x}),\Lambda_-(\mathbf{x}))$, $\Lambda_\pm(x) = V^{(1)}(x) \pm \phi^{(1)}(x)$ and $P_1 = I_2$. In practical computation, when $A_1(t,x) \not\equiv 0$, due to the fact that $\sigma_1\sigma_3 \neq \sigma_3\sigma_1$, we will split (3.5) into two steps as: one first solves

$$\partial_t\Psi(t,x) = -i\omega(V(t,x)I_2 - A_1(t,x)\sigma_1)\Psi(t,x), \quad x \in \Omega, \quad t > 0, \tag{3.11}$$

followed by solving

$$\partial_t \Psi(t,x) = -ig\phi(t,x)\sigma_3\Psi(t,x), \quad x \in \Omega, \quad t > 0. \tag{3.12}$$

In this case, integrating the splitting steps in time and combining them via the Strang splitting [2,38] result in

$$\Psi(t_{n+1},x) = e^{-iP_2\Lambda^{(1)}(x)P_2^*/2}e^{-i\phi^{(1)}(x)\sigma_3}e^{-iP_2\Lambda^{(1)}(x)P_2^*/2}\Psi(t_n,x), \quad x \in \Omega, \quad n \geq 0, \tag{3.13}$$

where $\Lambda^{(1)}(x) = \mathrm{diag}(\Lambda_+^{(1)}(\mathrm{x}), \Lambda_-^{(1)}(\mathrm{x}))$, $\Lambda_\pm^{(1)}(x) = V^{(1)}(x) \pm A_1^{(1)}(x)$, $A_1^{(1)}(x) = \omega \int_{t_n}^{t_{n+1}} A_1(t,x)dt$ and

$$P_2 = \begin{pmatrix} \dfrac{1}{\sqrt{2}} & \dfrac{1}{\sqrt{2}} \\ -\dfrac{1}{\sqrt{2}} & \dfrac{1}{\sqrt{2}} \end{pmatrix}. \tag{3.14}$$

Note that the integral $\phi^{(1)}(x)$ can be approximated via the following quadrature rule as

$$\phi^{(1)}(x) \approx g(\phi(t_n,x)\tau + \frac{1}{2}v(t_n,x)\tau^2).$$

In addition, if the definite integrals $V^{(1)}(x)$ and $A_1^{(1)}(x)$ cannot be evaluated analytically, we could evaluate them numerically via the Simpson's quadrature rule as

$$V^{(1)}(x) = \omega \int_{t_n}^{t_{n+1}} V(t,x)dt \approx \frac{\omega\tau}{6}\left[V(t_n,x) + 4V\left(t_n + \frac{\tau}{2}, x\right) + V(t_{n+1},x)\right],$$

$$A_1^{(1)}(x) = \omega \int_{t_n}^{t_{n+1}} A_1(t,x)dt \approx \frac{\omega\tau}{6}\left[A_1(t_n,x) + 4A_1\left(t_n + \frac{\tau}{2}, x\right) + A_1(t_{n+1},x)\right].$$

For the Klein-Gordon component, the solution to the ODE (3.6) is trivial by noticing it leaves $\phi(t,x)$ invariant in t and the ODE (3.7) can also be integrated from time t_n to t_{n+1} directly, we have

$$\phi(t_{n+1},x) = \phi(t_n,x), \quad v(t_{n+1},x) = v(t_n,x) + \frac{1}{\varepsilon^2}\int_{t_n}^{t_{n+1}} g\Psi^*(t,x)\sigma_3\Psi(t,x)dt, \quad x \in \Omega, \quad n \geq 0, \tag{3.15}$$

with the integral being approximated by the trapezoid quadrature rule as

$$v(t_{n+1},x) \approx v(t_n,x) + \frac{1}{2\varepsilon^2}\tau(H(t_n,x) + H(t_{n+1},x)), \quad \text{where} \quad H(t,x) = g\Psi^*(t,x)\sigma_3\Psi(t,x).$$

Now, the remained part is to find an efficient and accurate method for (3.4) and (3.8)-(3.9). In fact, we shall apply the Fourier spectral discretization in space and solve them in phase space exactly similar as in Section 2. Thus it results in finding $\Psi_M(t,x) \in Y_M$ and $(\phi_M(t,x), v_M(t,x)) \in [Z_M]^2$, i.e.,

$$\Psi_M(t,x) = \sum_{l \in \mathscr{T}_M} \widehat{(\Psi_M)}_l(t)e^{i\mu_l(x-a)}, \phi_M(t,x) = \sum_{l \in \mathscr{T}_M} \widehat{(\phi_M)}_l(t)e^{i\mu_l(x-a)}, v_M(t,x) = \sum_{l \in \mathscr{T}_M} \widehat{(v_M)}_l(t)e^{i\mu_l(x-a)},$$

satisfying

$$\widehat{(\Psi_M)}_l(t) = e^{-i\int_{t_n}^t \Gamma_l/\varepsilon^2 ds}\widehat{(\Psi_M)}_l(t_n) = e^{-i(t-t_n)\Gamma_l/\varepsilon^2}\widehat{(\Psi_M)}_l(t_n), \quad l \in \mathscr{T}_M, \tag{3.16}$$

$$\widehat{(\phi_M)}_l(t) = \cos(\beta_l(t-t_n))\widehat{(\phi_M)}_l(t_n) + \beta_l^{-1}\sin(\beta_l(t-t_n))\widehat{(v_M)}_l(t_n), \quad l \in \mathscr{T}_M, \tag{3.17}$$

$$\widehat{(v_M)}_l(t) = -\beta_l\sin(\beta_l(t-t_n))\widehat{(\phi_M)}_l(t_n) + \cos(\beta_l(t-t_n))\widehat{(v_M)}_l(t_n), \quad l \in \mathscr{T}_M, \tag{3.18}$$

where β_l and Γ_l are defined as in (2.11).

We observe that the Dirac field $\Psi_M(t_{n+1},x)$ could be obtained by the information of $\Psi_M(t_n,x)$, $\phi_M(t_n,x)$ and $v_M(t_n,x)$ only from the previous time step, while $v_M(t_{n+1},x)$ is identified by the information of $\Psi_M(t_n,x)$ and $\Psi_M(t_{n+1},x)$. Thus, in practical computation, at each time step, the computations of $\phi_M(t,x)$,

$v_M(t,x)$ and $\Psi_M(t,x)$ are decoupled. i.e., one first updates the Dirac field $\Psi_M(t,x)$ by solving (3.4) and (3.5), and then updates the Klein-Gordon field $(\phi_M(t,x), v_M(t,x))$ by solving (3.6)-(3.7) and (3.8)-(3.9). Similar as in Section 2, in order to overcome the difficulties for computing the Fourier coefficients, we adopt the Fourier pseudospectral discretization to replace the projections by the interpolations. Let $(\phi_j^n, v_j^n, \Psi_j^n)$ be the approximation of $(\phi(t_n, x_j), v(t_n, x_j), \Psi(t_n, x_j))$ and denote $\Psi^n \in X_M$, $\phi^n \in \widetilde{X}_M$ and $v^n \in \widetilde{X}_M$ be the solution vectors at $t_n = n\tau$ with components Ψ_j^n, ϕ_j^n and v_j^n ($j \in \mathscr{T}_M^0$ and $n \geq 0$), respectively. Choosing $\Psi_j^0 = \Psi^0(x_j)$, $\phi_j^0 = \phi^0(x_j)$ and $v_j^0 = \varepsilon^{-2} \gamma^0(x_j)$, combining the Fourier pseudospectral discretization with the splitting steps via the standard Strang splitting [2,6,22,38], which finally results a second order TSFP as

$$\Psi_j^{[1]} = \mathcal{L}_\Psi(\tau/2, \Psi^n)_j, \quad \Psi_j^{[2]} = S(x_j)\Psi_j^{[1]}, \quad \Psi_j^{n+1} = \mathcal{L}_\Psi(\tau/2, \Psi^{[2]})_j, \quad j \in \mathscr{T}_M^0, \quad n \geq 0, \qquad (3.19)$$

$$\phi_j^{[1]} = \phi_j^n, \quad v_j^{[1]} = v_j^n + \frac{1}{4\varepsilon^2}\tau(I_M H(t_n, x_j) + I_M H(t_{n+1}, x_j)), \quad j \in \mathscr{T}_M^0, \quad n \geq 0, \qquad (3.20)$$

$$\phi_j^{[2]} = \mathcal{L}_\phi(\tau, \phi^{[1]}, v^{[1]})_j, \quad v_j^{[2]} = \mathcal{L}_v(\tau, \phi^{[1]}, v^{[1]})_j, \quad j \in \mathscr{T}_M^0, \qquad (3.21)$$

$$\phi_j^{n+1} = \phi_j^{[2]}, \quad v_j^{n+1} = v_j^{[2]} + \frac{1}{4\varepsilon^2}\tau(I_M H(t_n, x_j) + I_M H(t_{n+1}, x_j)), \quad j \in \mathscr{T}_M^0, \quad n \geq 0, \qquad (3.22)$$

where

$$S(x) = \begin{cases} P_1 e^{-i\Lambda(x)} P_1^*, & \text{if } A_1(t,x) \equiv 0, \\ P_2 e^{-i\Lambda^{(1)}(x)/2} P_2^* e^{-i\phi^{(1)}(x)\sigma_3} P_2 e^{-i\Lambda^{(1)}(x)/2} P_2^*, & \text{if } A_1(t,x) \not\equiv 0, \end{cases} \qquad (3.23)$$

with $P_1 = I_2$, $\Lambda(x) = \mathrm{diag}(\Lambda_+(\mathrm{x}), \Lambda_-(\mathrm{x}))$, $\Lambda_\pm(x) = V^{(1)}(x) \pm \phi^{(1)}(x)$, $\phi^{(1)}(x) = g(\phi(t_n, x)\tau + \frac{1}{2}v(t_n, x)\tau^2)$, $\Lambda^{(1)}(x)$ and P_2 defined as in (3.14). $\mathcal{L}_\Psi(\tau, \Psi)_j$, $\mathcal{L}_\phi(\tau, \phi, v)_j$ and $\mathcal{L}_v(\tau, \phi, v)_j$ ($j \in \mathscr{T}_M^0$) are computed from any $\tau \in \mathbb{R}$, $\Psi \in X_M$, $\phi \in \widetilde{X}_M$ and $v \in \widetilde{X}_M$, which are defined as

$$\mathcal{L}_\Psi(\tau, \Psi)_j = \sum_{l \in \mathscr{T}_M} Q_l e^{-i\tau D_l/\varepsilon^2}(Q_l)^* \widetilde{\psi}_l e^{i\mu_l(x_j-a)},$$

$$\mathcal{L}_\phi(\tau, \phi, v)_j = \sum_{l \in \mathscr{T}_M} \left[\cos(\tau\beta_l)\widetilde{\phi}_l + \beta_l^{-1}\sin(\tau\beta_l)\widetilde{v}_l\right] e^{i\mu_l(x_j-a)},$$

$$\mathcal{L}_v(\tau, \phi, v)_j = \sum_{l \in \mathscr{T}_M} \left[-\beta_l \sin(\tau\beta_l)\widetilde{\phi}_l + \cos(\tau\beta_l)\widetilde{v}_l\right] e^{i\mu_l(x_j-a)},$$

with D_l and Q_l defined as in (2.12).

Similar to the discussion of the TSFP method for the (nonlinear) Dirac equation in [5,6], we can also get the following property. The proof is standard and simple, we omit it here for brevity.

Lemma 3.2 *The TSFP* (3.19)-(3.22) *conserves*

$$\|\Psi^n\|_{l^2}^2 := h \sum_{j \in \mathscr{T}_{M-1}^0} |\Psi_j^n|^2 \equiv h \sum_{j \in \mathscr{T}_{M-1}^0} |\Psi_j^0|^2 = \|\Psi^0\|_{l^2}^2, \quad n \geq 1, \qquad (3.24)$$

in the discretized level.

Followed on the Von Neumann linear stability analysis in [5,6,8], we could conclude that the TSFP (3.19)-(3.22) keeps the stability property for the KGD system, that is

Lemma 3.3 *For any* τ, $h > 0$ *and* $0 < \varepsilon \leq 1$, *the TSFP* (3.19)-(3.22) *is unconditionally stable.*

Finally, for benchmark comparisons, we propose another two alterative discretizations named DIFP-TSFP and GIFP-TSFP for short by applying the DIFP/GIFP method for the Klein-Gordon equation, while the TSFP method for the Dirac equation in the KGD (1.6), respectively. The details of the discretizations as follows:

(1). the DIFP-TSFP method reads

$$\Psi_j^{(1)} = \mathcal{L}_\Psi(\tau/2, \Psi^n)_j, \quad \Psi_j^{(2)} = S(x_j)\Psi_j^{(1)}, \quad \Psi_j^{n+1} = \mathcal{L}_\Psi(\tau/2, \Psi^{(2)})_j, \tag{3.25}$$

$$\phi_j^{n+1} = \sum_{l \in \mathscr{T}_M} \widetilde{\phi_l^{n+1}} e^{i\mu_l(x_j-a)}, \quad \upsilon_j^{n+1} = \sum_{l \in \mathscr{T}_M} \widetilde{\upsilon_l^{n+1}} e^{i\mu_l(x_j-a)}, \quad j \in \mathscr{T}_M^0, \quad n \geq 0, \tag{3.26}$$

satisfying

$$\widetilde{\phi_l^{n+1}} = p_l^{(1)} \widetilde{\phi_l^n} + q_l^{(1)} \widetilde{\upsilon_l^n} + \kappa_l^{(1)} \widetilde{H_l^n}, \quad \widetilde{\upsilon_l^{n+1}} = p_l^{(2)} \widetilde{\phi_l^n} + q_l^{(2)} \widetilde{\upsilon_l^n} + \kappa_l^{(2)} \widetilde{H_l^n} + \xi_l^{(2)} \widetilde{H_l^{n+1}}, \quad l \in \mathscr{T}_M, \tag{3.27}$$

where $S(x_j)$ is defined as (3.23) with $\phi^{(1)}(x_j) = g(\phi_j^n \tau + \frac{1}{2}\upsilon_j^n \tau^2)$, and the coefficients are given as in (2.25) - (2.26).

(2). the GIFP-TSFP method reads

$$\phi_j^{n+1} = \sum_{l \in \mathscr{T}_M} \widetilde{\phi}_l^{n+1} e^{i\mu_l(x_j-a)}, \quad \Psi_j^{(1)} = \mathcal{L}_\Psi(\tau/2, \Psi^n)_j, \quad j \in \mathscr{T}_M^0, \quad n \geq 0, \tag{3.28}$$

$$\Psi_j^{(2)} = S(x_j)\Psi_j^{(1)}, \quad \Psi_j^{n+1} = \mathcal{L}_\Psi(\tau/2, \Psi^{(2)})_j, \quad j \in \mathscr{T}_M^0, \quad n \geq 0, \tag{3.29}$$

satisfying

$$\widetilde{\phi}_l^1 = p_l^0 \widetilde{\phi}_l^0 + q_l^0 \widetilde{\gamma}_l + \kappa_l^0 \widetilde{H}_l^0(0) + \xi_l^0 (\widetilde{H_l^0})'(0), \quad \widetilde{\phi}_l^{n+1} = -\widetilde{\phi}_l^{n-1} + p_l^n \widetilde{\phi}_l^n + \kappa_l^n \widetilde{H}_l^n(0), \quad l \in \mathscr{T}_M, \tag{3.30}$$

where $S(x_j)$ is defined similar as (3.23) with $\phi^{(1)}(x_j) = g\tau(\phi_j^n + \phi_j^{n+1})/2$, and the coefficients are given as in (2.31) - (2.32).

The DIFP-TSFP (3.25)-(3.27) and GIFP-TSFP (3.28)-(3.30) are also unconditionally stable and keep the mass conservation law in the discretized level similar as the TSFP (3.19)-(3.22). In addition, the memory cost is $O(M)$ and the computational load per time step is $O(M\ln M)$ thanks to the FFT.

4 Numerical Comparison and Applications

In this section, we compare the accuracy of the numerical methods including the EWI-FP, TSFP, DIFP-TSFP and GIFP-TSFP methods to show their spatial/temporal resolution in terms of the singular perturbation ε, and then we display the dynamics of the KGD (1.6) in 2D with a honeycomb lattice potential for different ε under strong/weak interaction.

4.1 Spatial/Temporal resolution

In order to test the accuracy, the problem is solved numerically in 1D with the coefficients $g = 1$ and $\omega = 1$ on an large enough interval $\Omega = [-32, 32]$ with periodic boundary conditions. The 'reference' solution $(\phi(t,x), \Psi(t,x))$ is obtained numerically by using the TSFP (3.19)-(3.22) with a very small time step and a fine mesh size, e.g. $\tau_e = 5 \times 10^{-6}$ and $h_e = 1/1024$ for comparison.

Here, we test the spatial and temporal discretization errors with the initial data given as

$$\Psi^0(x) = (e^{-x^2/2}, e^{-(x-1)^2/2})^T, \quad \phi^0(x) = e^{-x^2/2}, \quad \gamma(x) = \frac{3}{2} e^{-x^2/2}, \tag{4.1}$$

and we mainly consider the following two potential cases:

Case I: free electromagnetic potential case, i.e., $V(t,x) = 0$ and $A_1(t,x) = 0$;

Case II: the electromagnetic potentials are chosen as

$$V(t,x) = (1-x)/(1+x^2), \quad A_1(t,x) = (x+1)^2/(1+x^2), \quad x \in \mathbb{R}, \quad t \geq 0. \tag{4.2}$$

Table 4.1: Spatial errors $e_\Psi^{\tau,h}$ (upper) and $e_\phi^{\tau,h}$ (lower) of TSFP with free electromagnetic potential.

Spatial errors	$h_0 = 4$	$h_0/2$	$h_0/2^2$	$h_0/2^3$	$h_0/2^4$
$\varepsilon_0 = 1$	6.12E-1	6.70E-1	1.66E-1	2.30E-3	4.79E-8
$\varepsilon_0/2$	9.90E-1	5.56E-1	6.14E-2	3.33E-4	2.02E-9
$\varepsilon_0/2^2$	8.32E-1	4.38E-1	2.42E-2	2.45E-5	6.22E-11
$\varepsilon_0/2^3$	7.74E-1	3.55E-1	1.17E-2	6.25E-6	5.76E-11
$\varepsilon_0/2^4$	7.13E-1	3.50E-1	1.16E-2	1.63E-6	5.74E-11
$\varepsilon_0/2^5$	7.15E-1	3.53E-1	1.21E-2	4.23E-7	5.75E-11
$\varepsilon_0 = 1$	1.14E+0	3.59E-1	6.25E-3	3.74E-5	1.60E-10
$\varepsilon_0/2$	2.57E-1	1.62E-1	2.02E-2	2.07E-5	5.11E-11
$\varepsilon_0/2^2$	1.24E-1	1.90E-1	3.65E-3	1.19E-6	2.50E-12
$\varepsilon_0/2^3$	9.57E-1	4.32E-1	1.25E-2	4.04E-7	1.37E-13
$\varepsilon_0/2^4$	1.15E+0	4.11E-1	1.06E-2	4.55E-8	4.49E-14
$\varepsilon_0/2^5$	5.03E-1	1.22E-1	9.51E-3	1.52E-8	7.84E-14

Table 4.2: Spatial errors $e_\Psi^{\tau,h}$ (upper) and $e_\phi^{\tau,h}$ (lower) of TSFP with the potentials (4.2).

Spatial errors	$h_0 = 4$	$h_0/2$	$h_0/2^2$	$h_0/2^3$	$h_0/2^4$
$\varepsilon_0 = 1$	8.82E-1	1.21E+0	6.07E-1	1.79E-1	1.33E-3
$\varepsilon_0/2$	1.15E+0	1.34E+0	5.52E-1	3.55E-2	5.85E-5
$\varepsilon_0/2^2$	9.36E-1	8.53E-1	3.45E-1	6.94E-3	1.09E-5
$\varepsilon_0/2^3$	8.23E-1	6.75E-1	2.10E-1	4.02E-3	5.66E-6
$\varepsilon_0/2^4$	9.10E-1	6.76E-1	2.13E-1	3.53E-3	3.70E-6
$\varepsilon_0/2^5$	1.00E+0	6.92E-1	2.19E-1	2.99E-3	2.50E-6
$\varepsilon_0 = 1$	8.64E-1	2.42E-1	3.93E-2	3.96E-3	1.07E-5
$\varepsilon_0/2$	4.54E-1	3.16E-1	6.72E-2	1.45E-3	6.31E-7
$\varepsilon_0/2^2$	1.28E-1	1.89E-1	1.10E-2	2.23E-4	2.41E-7
$\varepsilon_0/2^3$	9.65E-1	4.36E-1	1.44E-2	1.50E-5	1.56E-7
$\varepsilon_0/2^4$	1.14E+0	4.10E-1	9.96E-3	5.14E-6	4.69E-9
$\varepsilon_0/2^5$	5.03E-1	1.22E-1	9.69E-3	1.26E-6	4.09E-10

Denote $(\phi_{\tau,h}^n, \Psi_{\tau,h}^n)$ with the components (ϕ_j^n, Ψ_j^n) $(j \in \mathscr{T}_M^0)$ to be the numerical solution obtained by a numerical method with time step τ and mesh size h at the time $t = t_n$. In order to quantify the numerical results, we define the error function as

$$e_u^{\tau,h}(t_n) := \left(h \sum_{j \in \mathscr{T}_{M-1}^0} \left(|u(t_n, x_j) - u_j^n|^2 + |\delta_x^+(u(t_n, x_j) - u_j^n)|^2 \right) \right)^{1/2}, \quad u = \phi \text{ or } u = \Psi,$$

where $\delta_x^+ u_j^n = (u_{j+1}^n - u_j^n)/h$.

At first, we test the spatial errors with a very small time step (e.g. $\tau = \tau_e = 5 \times 10^{-6}$) under different mesh size h. Tables 4.1-4.2 list the spatial errors $e_\Psi^{\tau,h}(t)$ and $e_\phi^{\tau,h}(t)$ of the TSFP (3.19)-(3.22) at $t = 1$ with free electromagnetic potential and the electromagnetic potentials in (4.2), respectively. The spatial errors of other methods behave quite similarly to these of the TSFP method and we skip here for brevity. Then, for comparison, Tables 4.3-4.8 tabulate the temporal errors of the TSFP (3.19)-(3.22), GIFP-TSFP (3.28)-(3.30) and EWI-FP (2.22)-(2.24) at $t = 1$ for different τ and ε with $h = 1/32$, respectively. The results for the DIFP-TSFP (3.25)-(3.27) omitted here are similar to those of the TSFP and GIFP-TSFP methods.

From Tables 4.1-4.8 and additional results not shown here, we can draw the observations on different numerical methods for the KGD system:

(i). For the spatial resolution, the TSFP (3.19)-(3.22) converges optimally and uniformly with exponential convergence rate for any fixed $\varepsilon > 0$ (cf. each row in Tables 4.1-4.2). So do the EWI-FP (2.22)-(2.24), DIFP-TSFP (3.25)-(3.27) and GIFP-TSFP (3.28)-(3.30), due to the similar spatial discretization. The results suggest that the ε-scalability for the spatial discretizations is $h = O(1)$.

(ii). For the temporal resolution, in the $O(1)$ speed-of-light regime, i.e., $\varepsilon = O(1)$, the numerical methods are all second-order accurate (cf. the first row in Tables 4.3-4.8). In the nonrelativistic limit regime, i.e.,

Table 4.3: Temporal errors $e_\Psi^{\tau,h}$ (upper) and $e_\phi^{\tau,h}$ (lower) of TSFP with free electromagnetic potential.

Temporal errors	$\tau_0 = 0.2$	$\tau_0/4$	$\tau_0/4^2$	$\tau_0/4^3$	$\tau_0/4^4$	$\tau_0/4^5$
$\varepsilon_0 = 1$	2.57E+0	1.80E-3	1.12E-4	7.02E-6	4.39E-7	2.74E-8
order	-	5.24	2.00	2.00	2.00	2.00
$\varepsilon_0/2$	2.31E+0	5.97E-3	3.61E-4	2.24E-5	1.39E-6	8.70E-8
order	-	4.30	2.02	2.01	2.00	2.00
$\varepsilon_0/2^2$	2.31E+0	3.30E-2	1.83E-3	1.11E-4	6.85E-6	4.27E-7
order	-	3.07	2.09	2.02	2.01	2.00
$\varepsilon_0/2^3$	2.31E+0	8.92E-2	6.22E-3	3.99E-4	2.51E-5	1.57E-6
order	-	2.35	1.92	1.98	2.00	2.00
$\varepsilon_0/2^4$	2.30E+0	3.84E+0	3.41E-2	1.14E-3	6.27E-5	3.80E-6
order	-	-0.37	3.41	2.45	2.10	2.02
$\varepsilon_0/2^5$	2.31E+0	1.45E+0	4.46E-1	5.08E-3	1.89E-4	1.03E-5
order	-	0.34	0.84	3.23	2.37	2.10
$\varepsilon_0 = 1$	2.43E+0	9.85E-4	6.16E-5	3.85E-6	2.41E-7	1.50E-8
order	-	5.63	2.00	2.00	2.00	2.00
$\varepsilon_0/2$	2.55E+0	1.33E-3	8.38E-5	5.24E-6	3.27E-7	2.05E-8
order	-	5.45	2.00	2.00	2.00	2.00
$\varepsilon_0/2^2$	2.48E+0	6.24E-3	3.92E-4	2.44E-5	1.52E-6	9.50E-8
order	-	4.32	2.00	2.00	2.00	2.00
$\varepsilon_0/2^3$	2.46E+0	3.44E-2	1.79E-3	1.11E-4	6.94E-6	4.33E-7
order	-	3.08	2.13	2.00	2.00	2.00
$\varepsilon_0/2^4$	1.99E+0	2.34E-1	3.80E-3	1.98E-4	1.22E-5	7.60E-7
order	-	1.54	2.97	2.13	2.01	2.00
$\varepsilon_0/2^5$	1.98E+0	7.57E-2	6.39E-2	1.18E-3	6.07E-5	3.75E-6
order	-	2.36	0.12	2.88	2.14	2.01

Table 4.4: Temporal errors $e_\Psi^{\tau,h}$ (upper) and $e_\phi^{\tau,h}$ (lower) of TSFP with the potentials (4.2).

Temporal errors	$\tau_0 = 0.2$	$\tau_0/4$	$\tau_0/4^2$	$\tau_0/4^3$	$\tau_0/4^4$	$\tau_0/4^5$
$\varepsilon_0 = 1$	2.85E+0	3.79E-3	2.36E-4	1.48E-5	9.22E-7	5.76E-8
order	-	4.78	2.00	2.00	2.00	2.00
$\varepsilon_0/2$	2.86E+0	1.03E-2	6.46E-4	4.05E-5	2.53E-6	1.58E-7
order	-	4.06	2.00	2.00	2.00	2.00
$\varepsilon_0/2^2$	2.77E+0	4.31E-2	2.54E-3	1.59E-4	9.92E-6	6.20E-7
order	-	3.00	2.04	2.00	2.00	2.00
$\varepsilon_0/2^3$	2.70E+0	2.40E+0	1.22E-2	7.10E-4	4.42E-5	2.76E-6
order	-	0.08	3.81	2.05	2.00	2.00
$\varepsilon_0/2^4$	2.67E+0	3.44E+0	9.87E-1	3.44E-3	2.13E-4	1.34E-5
order	-	-0.18	0.90	4.08	2.01	1.99
$\varepsilon_0/2^5$	2.67E+0	1.99E+0	7.00E-1	2.34E-1	8.34E-4	5.00E-5
order	-	0.21	0.75	0.79	4.07	2.03
$\varepsilon_0 = 1$	2.34E+0	1.24E-3	7.78E-5	4.86E-6	3.04E-7	1.90E-8
order	-	5.44	2.00	2.00	2.00	2.00
$\varepsilon_0/2$	2.58E+0	3.00E-3	1.88E-4	1.18E-5	7.35E-7	4.59E-8
order	-	4.87	2.00	2.00	2.00	2.00
$\varepsilon_0/2^2$	2.49E+0	8.24E-3	5.25E-4	3.28E-5	2.04E-6	1.28E-7
order	-	4.12	1.99	2.00	2.00	2.00
$\varepsilon_0/2^3$	2.46E+0	2.43E-2	1.35E-3	8.72E-5	5.47E-6	3.42E-7
order	-	3.33	2.08	1.98	2.00	2.00
$\varepsilon_0/2^4$	1.99E+0	6.95E-1	5.98E-3	3.05E-4	1.88E-5	1.17E-6
order	-	0.76	3.43	2.15	2.01	2.00
$\varepsilon_0/2^5$	1.98E+0	8.18E-2	6.90E-2	9.90E-4	5.14E-5	3.18E-6
order	-	2.30	0.12	3.06	2.13	2.00

Table 4.5: Temporal errors $e_\Psi^{\tau,h}$ (upper) and $e_\phi^{\tau,h}$ (lower) of GIFP-TSFP with free electromagnetic potential.

Temporal errors	$\tau_0 = 0.2$	$\tau_0/4$	$\tau_0/4^2$	$\tau_0/4^3$	$\tau_0/4^4$	$\tau_0/4^5$
$\varepsilon_0 = 1$	2.57E+0	2.06E-3	1.29E-4	8.05E-6	5.03E-7	3.15E-8
order	-	5.14	2.00	2.00	2.00	2.00
$\varepsilon_0/2$	2.31E+0	4.40E-3	2.75E-4	1.72E-5	1.07E-6	6.72E-8
order	-	4.52	2.00	2.00	2.00	2.00
$\varepsilon_0/2^2$	2.31E+0	1.67E-2	1.05E-3	6.54E-5	4.09E-6	2.56E-7
order	-	3.56	2.00	2.00	2.00	2.00
$\varepsilon_0/2^3$	2.31E+0	6.73E-2	3.55E-3	2.21E-4	1.38E-5	8.63E-7
order	-	2.55	2.12	2.00	2.00	2.00
$\varepsilon_0/2^4$	2.30E+0	5.41E-1	9.34E-3	4.92E-4	3.05E-5	1.91E-6
order	-	1.05	2.93	2.12	2.01	2.00
$\varepsilon_0/2^5$	2.31E+0	7.16E-2	7.77E-2	1.58E-3	8.25E-5	5.13E-6
order	-	2.50	-0.06	2.81	2.13	2.00
$\varepsilon_0 = 1$	2.43E+0	3.79E-4	2.36E-5	1.48E-6	9.24E-8	6.09E-9
order	-	6.32	2.00	2.00	2.00	1.96
$\varepsilon_0/2$	2.55E+0	8.11E-4	5.02E-5	3.14E-6	1.96E-7	1.23E-8
order	-	5.81	2.01	2.00	2.00	2.00
$\varepsilon_0/2^2$	2.48E+0	2.66E-3	1.54E-4	9.55E-6	5.97E-7	3.73E-8
order	-	4.93	2.06	2.00	2.00	2.00
$\varepsilon_0/2^3$	2.46E+0	1.67E-1	3.40E-4	2.03E-5	1.27E-6	7.93E-8
order	-	1.94	4.47	2.03	2.00	2.00
$\varepsilon_0/2^4$	1.99E+0	2.38E-2	2.38E-2	2.73E-5	1.71E-6	1.07E-7
order	-	3.19	0.00	4.88	2.00	2.00
$\varepsilon_0/2^5$	1.98E+0	2.50E-3	2.11E-3	2.14E-3	2.14E-6	1.35E-7
order	-	4.82	0.12	-0.01	4.98	1.99

Table 4.6: Temporal errors $e_\Psi^{\tau,h}$ (upper) and $e_\phi^{\tau,h}$ (lower) of GIFP-TSFP with the potentials (4.2).

Temporal errors	$\tau_0 = 0.2$	$\tau_0/4$	$\tau_0/4^2$	$\tau_0/4^3$	$\tau_0/4^4$	$\tau_0/4^5$
$\varepsilon_0 = 1$	2.85E+0	6.28E-3	3.92E-4	2.45E-5	1.53E-6	9.58E-8
order	-	4.41	2.00	2.00	2.00	2.00
$\varepsilon_0/2$	2.86E+0	1.76E-2	1.10E-3	6.86E-5	4.29E-6	2.68E-7
order	-	3.67	2.00	2.00	2.00	2.00
$\varepsilon_0/2^2$	2.77E+0	7.46E-2	4.46E-3	2.78E-4	1.74E-5	1.09E-6
order	-	2.61	2.03	2.00	2.00	2.00
$\varepsilon_0/2^3$	2.70E+0	2.33E+0	1.87E-2	1.12E-3	6.95E-5	4.34E-6
order	-	0.11	3.48	2.03	2.00	2.00
$\varepsilon_0/2^4$	2.67E+0	1.19E+0	9.64E-1	4.12E-3	2.46E-4	1.53E-5
order	-	0.59	0.15	3.93	2.03	2.00
$\varepsilon_0/2^5$	2.67E+0	1.93E-1	2.40E-1	2.31E-1	9.34E-4	5.58E-5
order	-	1.89	-0.16	0.03	3.97	2.03
$\varepsilon_0 = 1$	2.34E+0	8.54E-4	5.32E-5	3.33E-6	2.08E-7	1.31E-8
order	-	5.71	2.00	2.00	2.00	2.00
$\varepsilon_0/2$	2.58E+0	1.90E-3	1.17E-4	7.31E-6	4.57E-7	2.86E-8
order	-	5.20	2.01	2.00	2.00	2.00
$\varepsilon_0/2^2$	2.49E+0	3.38E-3	1.81E-4	1.12E-5	7.01E-7	4.38E-8
order	-	4.76	2.11	2.01	2.00	2.00
$\varepsilon_0/2^3$	2.46E+0	1.86E-1	5.70E-4	3.26E-5	2.02E-6	1.27E-7
order	-	1.86	4.17	2.06	2.00	2.00
$\varepsilon_0/2^4$	1.99E+0	2.34E-2	2.09E-2	2.05E-5	1.27E-6	7.91E-8
order	-	3.21	0.08	4.99	2.01	2.00
$\varepsilon_0/2^5$	1.98E+0	2.76E-3	2.35E-3	2.13E-3	3.13E-6	1.73E-7
order	-	4.75	0.12	0.07	4.71	2.08

Table 4.7: Temporal errors $e_\Psi^{\tau,h}$ (upper) and $e_\phi^{\tau,h}$ (lower) of EWI-FP with free electromagnetic potential.

Temporal errors	$\tau_0 = 0.2$	$\tau_0/4$	$\tau_0/4^2$	$\tau_0/4^3$	$\tau_0/4^4$	$\tau_0/4^5$
$\varepsilon_0 = 1$	2.57E+0	2.27E-2	1.44E-3	9.03E-5	5.65E-6	3.53E-7
order	-	3.41	1.99	2.00	2.00	2.00
$\varepsilon_0/2$	<u>2.31E+0</u>	6.60E-2	4.14E-3	2.58E-4	1.61E-5	1.01E-6
order	-	2.57	2.00	2.00	2.00	2.00
$\varepsilon_0/2^2$	2.31E+0	<u>2.51E-1</u>	1.74E-2	1.10E-3	6.87E-5	4.29E-6
order	-	1.60	1.93	1.99	2.00	2.00
$\varepsilon_0/2^3$	2.31E+0	1.38E-1	<u>3.98E-2</u>	3.05E-3	1.98E-4	1.25E-5
order	-	2.03	0.89	1.85	1.97	1.99
$\varepsilon_0/2^4$	2.30E+0	1.70E-1	5.78E-2	<u>1.14E-2</u>	7.83E-4	4.87E-5
order	-	1.88	0.78	1.17	1.93	2.00
$\varepsilon_0/2^5$	2.31E+0	1.76E-1	4.34E-2	1.17E-2	<u>1.29E-3</u>	9.48E-5
order	-	1.85	1.01	0.94	1.59	1.88
$\varepsilon_0 = 1$	2.43E+0	1.81E-3	1.09E-4	6.74E-6	4.20E-7	2.62E-8
order	-	5.20	2.03	2.01	2.00	2.00
$\varepsilon_0/2$	<u>2.55E+0</u>	8.25E-3	6.40E-4	4.20E-5	2.65E-6	1.66E-7
order	-	4.14	1.84	1.97	1.99	2.00
$\varepsilon_0/2^2$	2.48E+0	<u>3.55E-2</u>	1.45E-3	9.89E-5	6.42E-6	4.05E-7
order	-	3.06	2.31	1.94	1.97	1.99
$\varepsilon_0/2^3$	2.46E+0	7.00E-2	<u>6.76E-3</u>	5.13E-4	3.49E-5	2.22E-6
order	-	2.57	1.69	1.86	1.94	1.99
$\varepsilon_0/2^4$	1.99E+0	1.23E-1	8.90E-3	<u>1.74E-3</u>	1.71E-4	1.12E-5
order	-	2.01	1.90	1.18	1.68	1.96
$\varepsilon_0/2^5$	1.98E+0	4.27E-2	5.01E-2	1.97E-3	<u>6.72E-4</u>	3.49E-5
order	-	2.77	-0.11	2.33	0.77	2.13

Table 4.8: Temporal errors $e_\Psi^{\tau,h}$ (upper) and $e_\phi^{\tau,h}$ (lower) of EWI-FP with the potentials (4.2).

Temporal errors	$\tau_0 = 0.2$	$\tau_0/4$	$\tau_0/4^2$	$\tau_0/4^3$	$\tau_0/4^4$	$\tau_0/4^5$
$\varepsilon_0 = 1$	2.85E+0	8.42E-2	5.27E-3	3.31E-4	2.07E-5	1.30E-6
order	-	2.54	2.00	2.00	2.00	2.00
$\varepsilon_0/2$	<u>2.86E+0</u>	1.79E-1	1.09E-2	6.78E-4	4.24E-5	2.65E-6
order	-	2.00	2.00	2.00	2.00	2.00
$\varepsilon_0/2^2$	2.77E+0	<u>9.42E-1</u>	5.31E-2	3.31E-3	2.07E-4	1.29E-5
order	-	0.78	2.08	2.00	2.00	2.00
$\varepsilon_0/2^3$	2.70E+0	7.11E+0	<u>5.96E-1</u>	3.70E-2	2.32E-3	1.45E-4
order	-	-0.70	1.79	2.00	2.00	2.00
$\varepsilon_0/2^4$	2.67E+0	1.94E+0	6.51E+0	<u>5.42E-1</u>	3.40E-2	2.13E-3
order	-	0.23	-0.87	1.79	2.00	2.00
$\varepsilon_0/2^5$	2.67E+0	1.85E+0	1.87E+0	6.03E+0	<u>5.32E-1</u>	3.35E-2
order	-	0.26	-0.01	-0.84	1.75	2.00
$\varepsilon_0 = 1$	2.34E+0	3.33E-3	1.72E-4	1.05E-5	6.54E-7	4.09E-8
order	-	4.73	2.13	2.02	2.00	2.00
$\varepsilon_0/2$	<u>2.58E+0</u>	1.84E-2	1.35E-3	8.97E-5	5.69E-6	3.57E-7
order	-	3.56	1.89	1.96	1.99	2.00
$\varepsilon_0/2^2$	2.49E+0	<u>8.40E-2</u>	2.19E-3	1.37E-4	8.86E-6	5.59E-7
order	-	2.45	2.63	2.00	1.98	1.99
$\varepsilon_0/2^3$	2.46E+0	1.79E-1	<u>6.46E-3</u>	4.04E-4	2.46E-5	1.53E-6
order	-	1.89	2.40	2.00	2.02	2.01
$\varepsilon_0/2^4$	1.99E+0	1.23E-1	3.75E-2	<u>2.26E-3</u>	1.52E-4	1.07E-5
order	-	2.01	0.86	2.03	1.95	1.92
$\varepsilon_0/2^5$	1.98E+0	4.30E-2	5.02E-2	5.11E-3	<u>4.55E-4</u>	2.89E-5
order	-	2.76	-0.11	1.65	1.75	1.99

$0 < \varepsilon \ll 1$, as ε vanishes, all the methods are second-order accurate in time when τ is sufficiently small, i.e., within the convergence regime, e.g. $\tau \lesssim \varepsilon^2$, (cf. the upper triangles above the diagonals in Tables 4.3-4.8), and all methods either have some convergence order reductions or lose the convergence outside the convergence regime (cf. the lower triangles below the diagonals in Tables 4.3-4.8). Among the four numerical methods, the TSFP-type methods (i.e., TSFP (3.19)-(3.22), DIFP-TSFP (3.25)-(3.27) and GIFP-TSFP (3.28)-(3.30)) always offer better temporal approximations than the EWI-FP (2.22)-(2.24) under the same time step, especially when ε becomes small (cf. each column in Tables 4.3-4.8).

4.2 Comparisons on physical observables and ε-scalability

In order to compare the numerical methods on the approximations of some physical observables for the KGD system, define the errors of the density and the current as

$$e_\rho^{\tau,h}(t_n) := h \sum_{j \in \mathscr{T}_{M-1}^0} |\rho(t_n, x_j) - \rho_j^n|, \quad e_{\mathcal{J}}^{\tau,h}(t_n) := h \sum_{j \in \mathscr{T}_{M-1}^0} |\mathcal{J}(t_n, x_j) - \mathcal{J}_j^n|, \tag{4.3}$$

where the density $\rho^n = |\Psi_{\tau,h}^n|^2$ and the current $\mathcal{J}^n = \frac{1}{\varepsilon}(\Psi_{\tau,h}^n)^* \sigma_1 \Psi_{\tau,h}^n$. Tables 4.9-4.10 show the temporal errors $e_\rho^{\tau,h}(t = 1)$ and $e_{\mathcal{J}}^{\tau,h}(t = 1)$ of the TSFP and EWI-FP methods with the electromagnetic potentials (4.2) for different τ and $h = 1/32$, respectively. The other two methods are similar to the TSFP method. On the other hand, Table 4.11 depicts the performance of the EWI-FP, TSFP, DIFP-TSFP and GIFP-TSFP methods in temporal approximations under the meshing strategy $\tau = O(\varepsilon^2)$. While Figure 4.2 shows the dependence of the temporal discretization error $e_\Psi^{\tau,h}(t) + e_\phi^{\tau,h}(t)$ on ε in log-scale for different τ at $t = 1$ under $h = 1/32$.

From Tables 4.9-4.11, Figure 4.2 and additional results not shown here, we can draw the observations:

(i). the temporal errors $e_\rho^{\tau,h}(t = 1)$ and $e_{\mathcal{J}}^{\tau,h}(t = 1)$ of the numerical methods all have second order convergent rate at $O(\tau^2)$ when $\tau \lesssim \varepsilon^2$ (cf. the upper parts of Tables 4.9-4.10). In addition, the TSFP, DIFP-TSFP and GIFP-TSFP methods perform much better than the EWI-FP method at a fixed time step (cf. each column in Tables 4.9-4.10) and under the ε-scalability at $\tau = O(\varepsilon^2)$ in the nonrelativistic limit regime (cf. diagonal lines in Tables 4.9-4.10).

(ii). Table 4.11 illustrates that the EWI-FP method shows no convergence in terms of ε under the mesh strategy $\tau = O(\varepsilon^2)$ as $\varepsilon \to 0$, while the other methods are convergent. Furthermore, Figure 4.2 indicates that the bounds of temporal discretization errors for the TSFP, DIFP-TSFP and GIFP-TSFP methods within the convergence regime behave like $O(\varepsilon^{-2}\tau^2)$ (cf. (a), (b) and (c)), while that of the EWI-FP method would asymptotically behave like $O(\varepsilon^{-4}\tau^2)$ (cf. (d)).

4.3 Dynamics in 2D with a honeycomb lattice potential

In this subsection, we study numerically about the dynamics of the KGD (1.6) in 2D with a honeycomb lattice potential, i.e., we take $d = 2$ and

$$A_1(t, \mathbf{x}) = A_2(t, \mathbf{x}) \equiv 0, \quad V(t, \mathbf{x}) = \cos\left(\frac{4\pi}{\sqrt{3}}\mathbf{e}_1 \cdot \mathbf{x}\right) + \cos\left(\frac{4\pi}{\sqrt{3}}\mathbf{e}_2 \cdot \mathbf{x}\right) + \cos\left(\frac{4\pi}{\sqrt{3}}\mathbf{e}_3 \cdot \mathbf{x}\right), \tag{4.4}$$

with

$$\mathbf{e}_1 = (-1, 0)^T, \quad \mathbf{e}_2 = (1/2, \sqrt{3}/2)^T, \quad \mathbf{e}_3 = (1/2, -\sqrt{3}/2)^T. \tag{4.5}$$

The initial data is taken as

$$\Psi^0(x) = (e^{-(x_1^2+x_2^2)/2}, e^{-((x_1-1)^2+x_2^2)/2})^T, \quad \phi^0(x) = e^{-(x_1^2+x_2^2)/2}, \quad \gamma(x) = \frac{3}{2}e^{-(x_1^2+x_2^2)/2}. \tag{4.6}$$

The problem is solved numerically on $\Omega = [-10, 10]^2$ by the TSFP, DIFP-TSFP or GIFP-TSFP method with the mesh size $h = 1/16$ and time step $\tau = 0.0001$. Figures 4.3-4.8 depict various dynamics of the

Table 4.9: Temporal errors $e_\rho^{\tau,h}$ (upper) and $e_{\mathcal{J}}^{\tau,h}$ (lower) of TSFP with the potentials (4.2).

Temporal errors	$\tau_0 = 0.2$	$\tau_0/4$	$\tau_0/4^2$	$\tau_0/4^3$	$\tau_0/4^4$	$\tau_0/4^5$
$\varepsilon_0 = 1$	<u>3.54E+0</u>	2.82E-3	1.77E-4	1.10E-5	6.90E-7	4.31E-8
order	-	5.15	2.00	2.00	2.00	2.00
$\varepsilon_0/2$	3.54E+0	<u>1.05E-2</u>	6.58E-4	4.11E-5	2.57E-6	1.61E-7
order	-	4.20	2.00	2.00	2.00	2.00
$\varepsilon_0/2^2$	3.54E+0	2.56E-2	<u>1.54E-3</u>	9.63E-5	6.02E-6	3.76E-7
order	-	3.56	2.02	2.00	2.00	2.00
$\varepsilon_0/2^3$	3.54E+0	5.65E-1	5.69E-3	<u>3.43E-4</u>	2.14E-5	1.33E-6
order	-	1.33	3.32	2.03	2.00	2.00
$\varepsilon_0/2^4$	3.54E+0	4.98E-1	1.25E-1	8.69E-4	<u>5.27E-5</u>	3.29E-6
order	-	1.42	0.99	3.59	2.02	2.00
$\varepsilon_0/2^5$	3.54E+0	1.20E-1	1.37E-1	2.19E-2	2.07E-4	<u>1.26E-5</u>
order	-	2.44	-0.10	1.32	3.36	2.02
$\varepsilon_0 = 1$	<u>2.11E+0</u>	2.03E-3	1.27E-4	7.92E-6	4.95E-7	3.09E-8
order	-	5.01	2.00	2.00	2.00	2.00
$\varepsilon_0/2$	4.00E+0	<u>1.97E-2</u>	1.22E-3	7.64E-5	4.78E-6	2.99E-7
order	-	3.83	2.01	2.00	2.00	2.00
$\varepsilon_0/2^2$	5.56E+0	1.42E-1	<u>8.51E-3</u>	5.31E-4	3.32E-5	2.07E-6
order	-	2.64	2.03	2.00	2.00	2.00
$\varepsilon_0/2^3$	7.72E+0	1.79E+1	1.22E-1	<u>7.13E-3</u>	4.44E-4	2.77E-5
order	-	-0.61	3.60	2.05	2.00	2.00
$\varepsilon_0/2^4$	1.12E+1	1.73E+1	1.94E+1	5.47E-2	<u>3.19E-3</u>	1.99E-4
order	-	-0.31	-0.09	4.24	2.05	2.00
$\varepsilon_0/2^5$	2.03E+1	2.14E+0	2.06E+0	2.47E+0	6.86E-3	<u>4.08E-4</u>
order	-	1.62	0.03	-0.13	4.25	2.04

Table 4.10: Temporal errors $e_\rho^{\tau,h}$ (upper) and $e_{\mathcal{J}}^{\tau,h}$ (lower) of EWI-FP with the potentials (4.2).

Temporal errors	$\tau_0 = 0.2$	$\tau_0/4$	$\tau_0/4^2$	$\tau_0/4^3$	$\tau_0/4^4$	$\tau_0/4^5$
$\varepsilon_0 = 1$	<u>3.54E+0</u>	3.40E-2	2.07E-3	1.31E-4	8.21E-6	5.14E-7
order	-	3.35	2.02	1.99	2.00	2.00
$\varepsilon_0/2$	3.54E+0	<u>1.58E-1</u>	1.03E-2	6.55E-4	4.12E-5	2.58E-6
order	-	2.24	1.97	1.98	2.00	2.00
$\varepsilon_0/2^2$	3.54E+0	8.72E-1	<u>2.94E-2</u>	2.19E-3	1.43E-4	9.05E-6
order	-	1.01	2.44	1.87	1.97	1.99
$\varepsilon_0/2^3$	3.54E+0	1.58E+1	4.22E-1	<u>7.82E-3</u>	3.86E-4	2.39E-5
order	-	-1.08	2.61	2.88	2.17	2.01
$\varepsilon_0/2^4$	3.54E+0	3.58E-1	1.62E+1	2.81E-1	<u>7.14E-3</u>	3.85E-4
order	-	1.65	-2.75	2.93	2.65	2.11
$\varepsilon_0/2^5$	3.54E+0	4.53E-1	1.50E-1	1.44E+1	2.73E-1	<u>7.22E-3</u>
order	-	1.48	0.80	-3.29	2.86	2.62
$\varepsilon_0 = 1$	<u>2.11E+0</u>	2.98E-2	1.76E-3	1.10E-4	6.91E-6	4.32E-7
order	-	3.07	2.04	2.00	2.00	2.00
$\varepsilon_0/2$	4.00E+0	<u>1.66E-1</u>	1.13E-2	7.36E-4	4.65E-5	2.92E-6
order	-	2.30	1.94	1.97	1.99	2.00
$\varepsilon_0/2^2$	5.56E+0	7.78E-2	<u>4.74E-3</u>	2.99E-4	1.88E-5	1.17E-6
order	-	3.08	2.02	1.99	2.00	2.00
$\varepsilon_0/2^3$	7.72E+0	1.36E+2	5.64E+0	<u>1.06E-1</u>	5.88E-3	3.85E-4
order	-	-2.07	2.30	2.86	2.09	1.97
$\varepsilon_0/2^4$	1.12E+1	1.29E+1	2.90E+2	9.33E+0	<u>1.84E-1</u>	1.31E-2
order	-	-0.11	-2.24	2.48	2.83	1.90
$\varepsilon_0/2^5$	2.03E+1	2.92E+1	2.97E+1	5.16E+2	1.72E+1	<u>3.82E-1</u>
order	-	-0.26	-0.01	-2.06	2.45	2.75

Table 4.11: Comparison of temporal errors $e_\Psi^{\tau,h}$ (upper) and $e_\phi^{\tau,h}$ (lower) with the potentials (4.2).

ε-scalability	$\varepsilon_0 = 0.5$	$\varepsilon_0/2$	$\varepsilon_0/2^2$	$\varepsilon_0/2^3$	$\varepsilon_0/2^4$
$\tau = O(\varepsilon^2)$	$\tau_0 = 0.2$	$\tau_0/4$	$\tau_0/4^2$	$\tau_0/4^3$	$\tau_0/4^4$
TSFP	2.86E+0	4.31E-2	1.22E-2	3.44E-3	8.34E-4
order	-	3.03	0.91	0.91	1.02
DIFP-TSFP	2.86E+0	4.28E-2	1.21E-2	3.43E-3	8.34E-4
order	-	3.03	0.91	0.91	1.02
GIFP-TSFP	2.86E+0	7.46E-2	1.87E-2	4.12E-3	9.34E-4
order	-	2.63	1.00	1.09	1.07
EWI-FP	2.86E+0	9.42E-1	5.96E-1	5.42E-1	5.32E-1
order	-	0.80	0.33	0.07	0.01
TSFP	2.58E+0	8.24E-3	1.35E-3	3.05E-4	5.14E-5
order	-	4.15	1.30	1.07	1.28
DIFP-TSFP	2.58E+0	7.18E-3	1.27E-3	3.04E-4	5.11E-5
order	-	4.24	1.25	1.03	1.29
GIFP-TSFP	2.58E+0	3.38E-3	5.70E-4	2.05E-5	3.13E-6
order	-	4.79	1.28	2.40	1.36
EWI-FP	2.58E+0	8.40E-2	6.46E-3	2.26E-3	4.55E-4
order	-	2.47	1.83	0.76	1.16
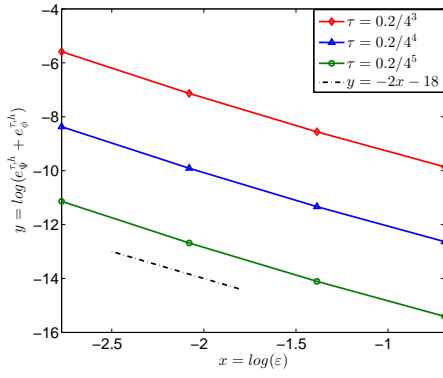
(a) TSFP
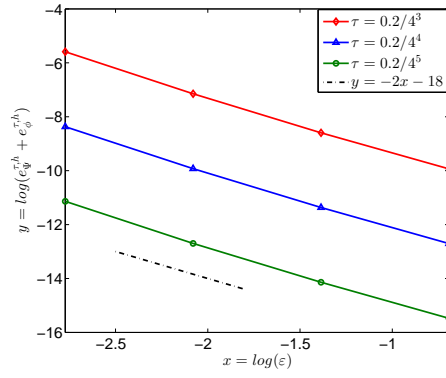
(b) DIFP-TSFP
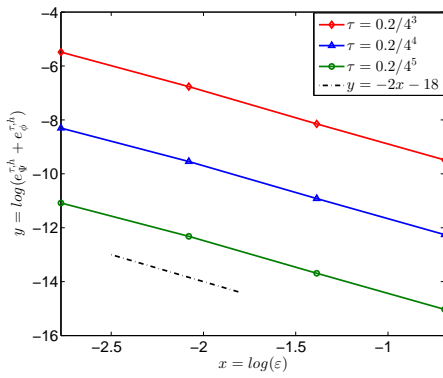
(c) GIFP-TSFP
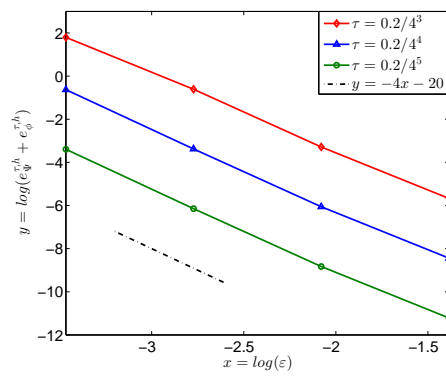
(d) EWI-FP

Fig. 4.2: Dependence of the temporal discretization error $e_\Psi^{\tau,h} + e_\phi^{\tau,h}$ on ε in log-scale for different τ at $t = 1$ under $h = 1/32$: (a) for TSFP, (b) for DIFP-TSFP, (c) for GIFP-TSFP and (d) for EWI-FP.
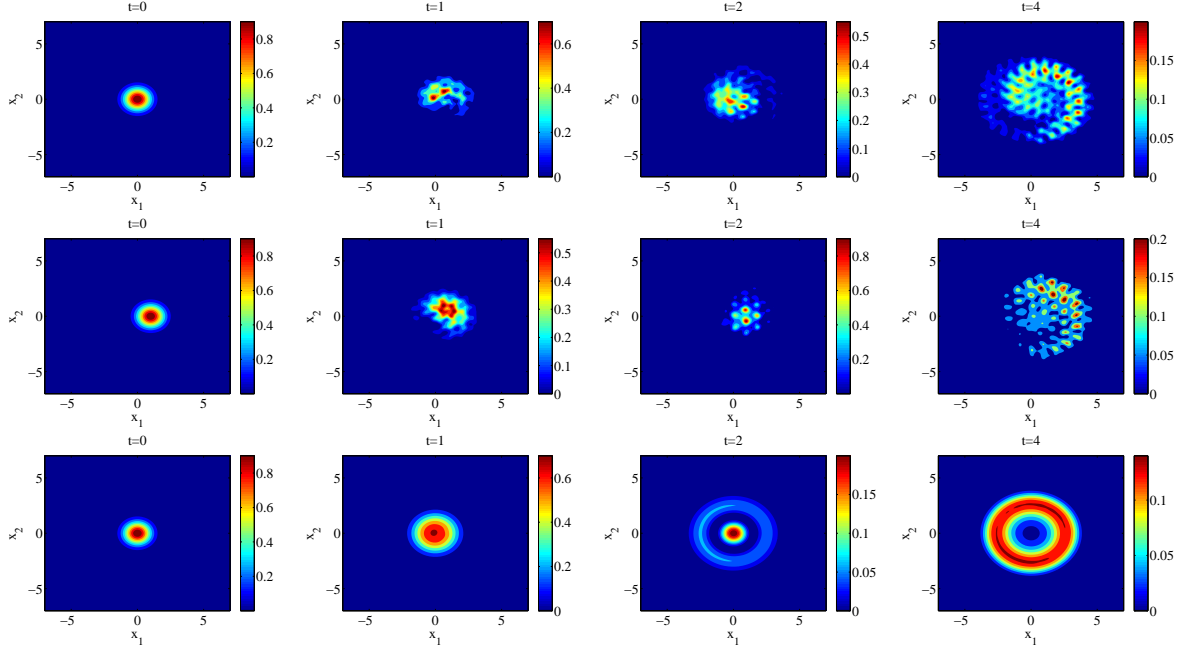
Fig. 4.3: Dynamics of the densities $\rho_1(t,\mathbf{x}) = |\psi_1(t,\mathbf{x})|^2$ (first row), $\rho_2(t,\mathbf{x}) = |\psi_2(t,\mathbf{x})|^2$ (second row) and $\rho_3(t,\mathbf{x}) = |\phi(t,\mathbf{x})|^2$ (third row) of the KGD system in 2D with a honeycomb potential, when $\varepsilon = 1$ and $g = 0.1$.
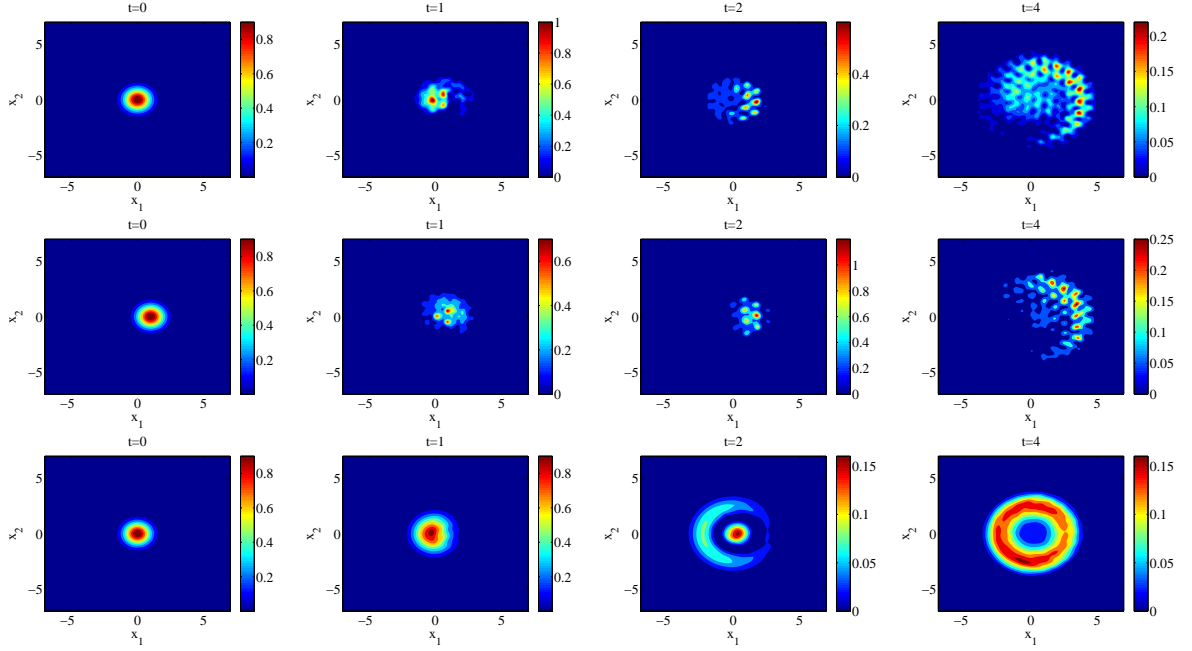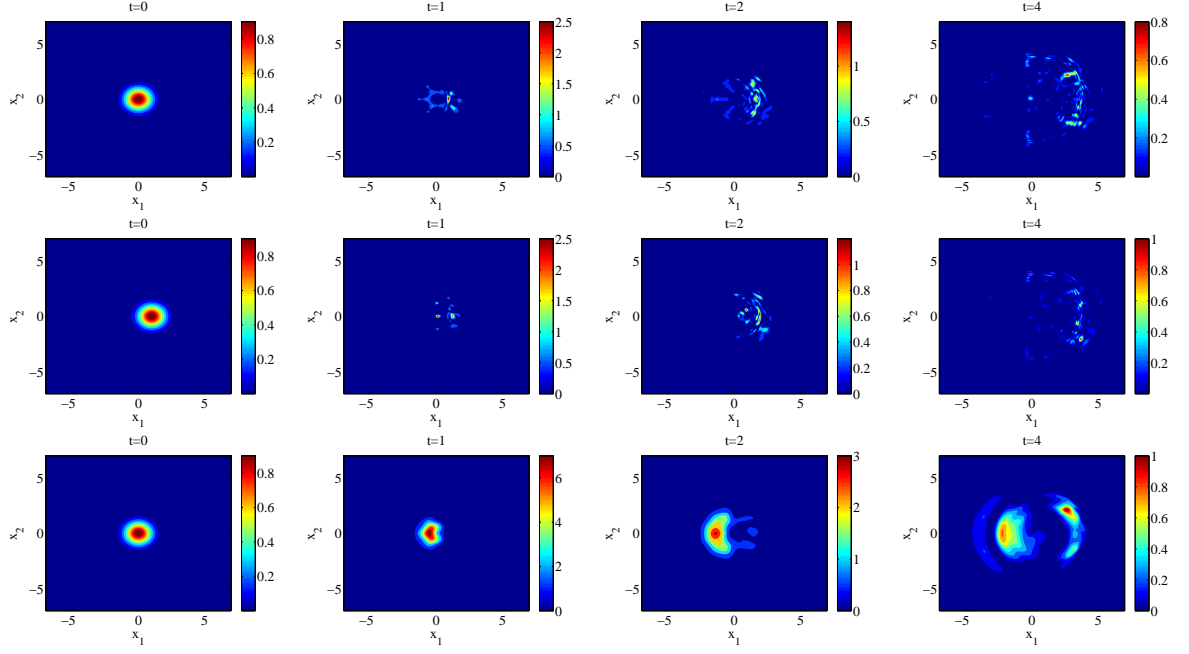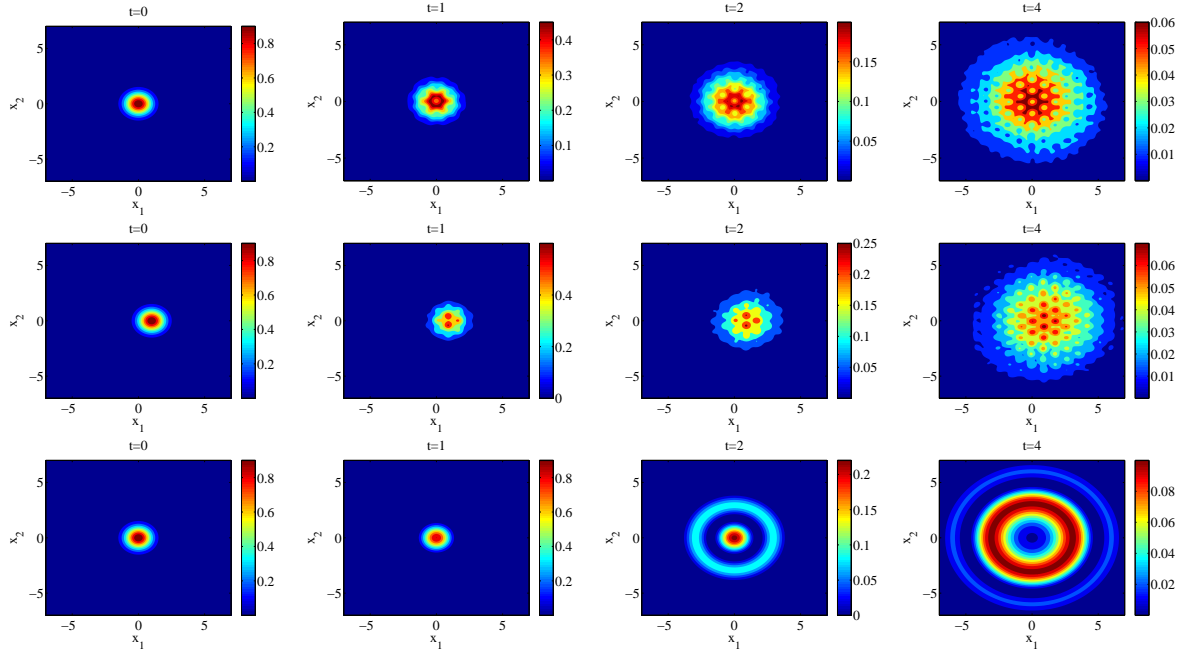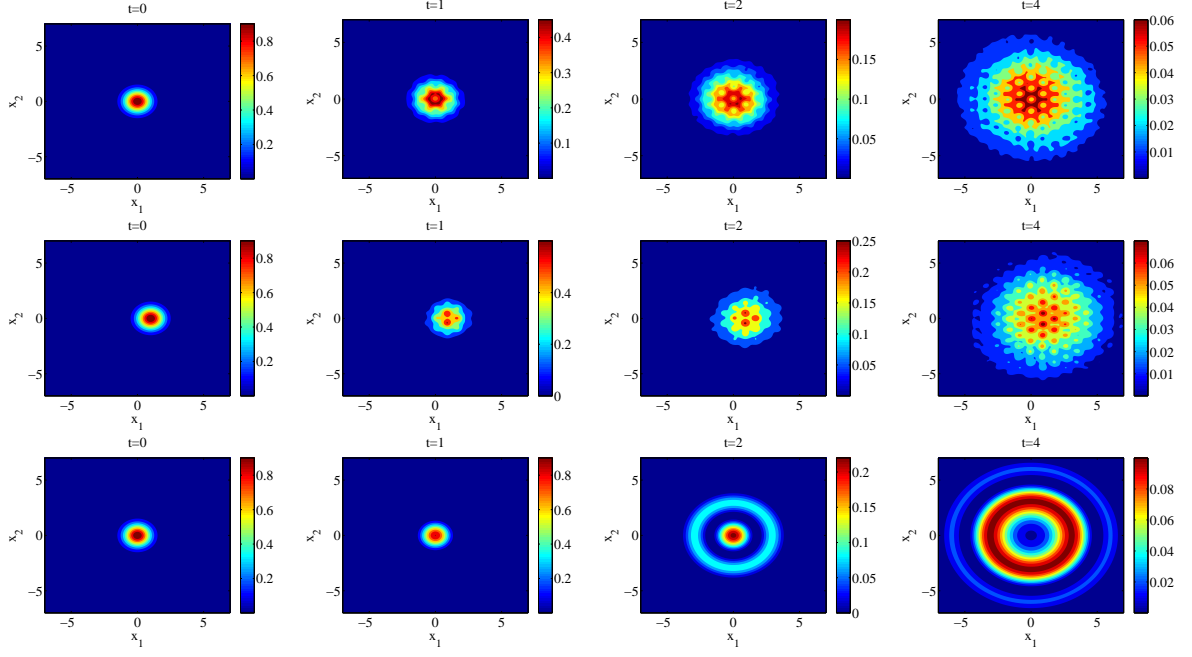

Fig. 4.4: Dynamics of the densities $\rho_1(t,\mathbf{x}) = |\psi_1(t,\mathbf{x})|^2$ (first row), $\rho_2(t,\mathbf{x}) = |\psi_2(t,\mathbf{x})|^2$ (second row) and $\rho_3(t,\mathbf{x}) = |\phi(t,\mathbf{x})|^2$ (third row) of the KGD system in 2D with a honeycomb potential, when $\varepsilon = 1$ and $g = 1$.

Fig. 4.5: Dynamics of the densities $\rho_1(t,\mathbf{x}) = |\psi_1(t,\mathbf{x})|^2$ (first row), $\rho_2(t,\mathbf{x}) = |\psi_2(t,\mathbf{x})|^2$ (second row) and $\rho_3(t,\mathbf{x}) = |\phi(t,\mathbf{x})|^2$ (third row) of the KGD system in 2D with a honeycomb potential, when $\varepsilon = 1$ and $g = 10$.

Fig. 4.6: Dynamics of the densities $\rho_1(t,\mathbf{x}) = |\psi_1(t,\mathbf{x})|^2$ (first row), $\rho_2(t,\mathbf{x}) = |\psi_2(t,\mathbf{x})|^2$ (second row) and $\rho_3(t,\mathbf{x}) = |\phi(t,\mathbf{x})|^2$ (third row) of the KGD system in 2D with a honeycomb potential, when $\varepsilon = 0.1$ and $g = 0.1$.
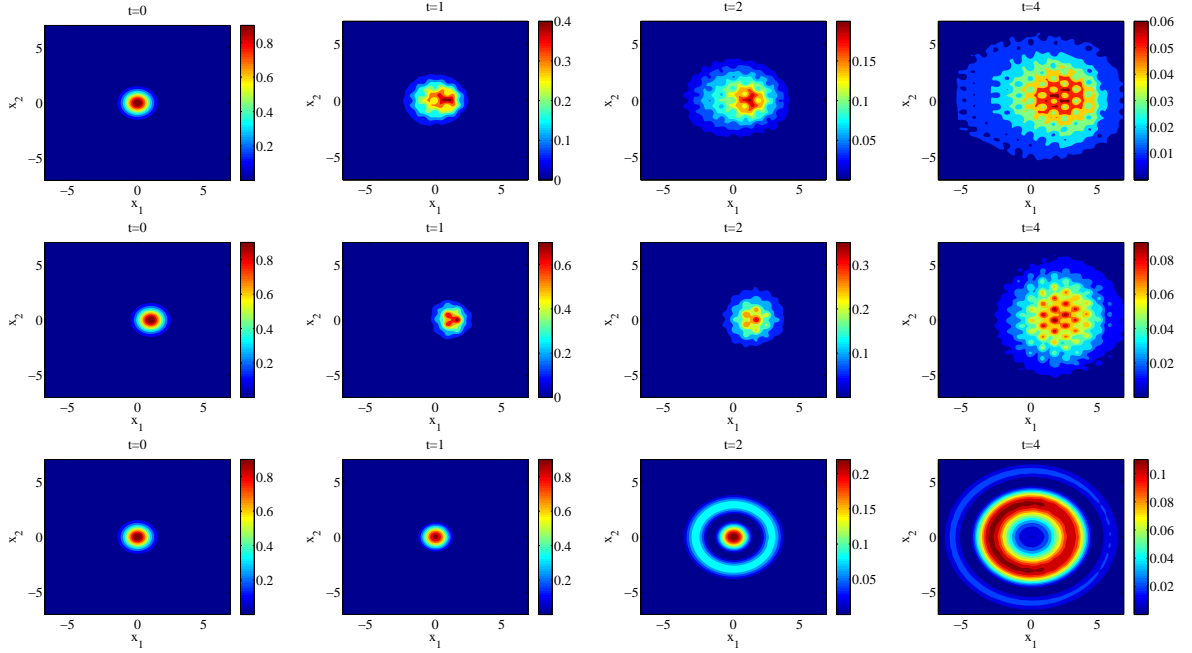
Fig. 4.7: Dynamics of the densities $\rho_1(t,\mathbf{x}) = |\psi_1(t,\mathbf{x})|^2$ (first row), $\rho_2(t,\mathbf{x}) = |\psi_2(t,\mathbf{x})|^2$ (second row) and $\rho_3(t,\mathbf{x}) = |\phi(t,\mathbf{x})|^2$ (third row) of the KGD system in 2D with a honeycomb potential, when $\varepsilon = 0.1$ and $g = 1$.

Fig. 4.8: Dynamics of the densities $\rho_1(t,\mathbf{x}) = |\psi_1(t,\mathbf{x})|^2$ (first row), $\rho_2(t,\mathbf{x}) = |\psi_2(t,\mathbf{x})|^2$ (second row) and $\rho_3(t,\mathbf{x}) = |\phi(t,\mathbf{x})|^2$ (third row) of the KGD system in 2D with a honeycomb potential, when $\varepsilon = 0.1$ and $g = 10$.

densities $\rho_j(t, \mathbf{x}) = |\psi_j(t, \mathbf{x})|^2$ $(j = 1, 2)$ and $\rho_3(t, \mathbf{x}) = |\phi(t, \mathbf{x})|^2$ for $\varepsilon = 1$ and $\varepsilon = 0.1$ with different interaction coefficients $g = 0.1, 1, 10$, respectively.

From Figures 4.3-4.8, we could observe that the dynamics of the KGD system depend greatly on the singular perturbation ε and the weak/strong interaction. For $\varepsilon = 1$, the dynamics of the densities are fluctuating in a random pattern, featured as quantum Zitterbewequng [21]. In addition, as ε decreases, the relativistic effects will vanish, the densities spread over in a smoother way.

5 Conclusion

Four optimal resolution discretizations based on the EWI-FP and TSFP methods were proposed and compared for solving the KGD system in the nonrelativistic limit regime. The numerical results indicate that the four specific discretizations are all of second-order temporal accuracy when $\tau \lesssim \varepsilon^2$ and uniform spectral spatial accuracy, which are superior than the FDTD methods. In addition, from the comparison of the temporal/spatial resolution and the ε-scalability, the TSFP-type methods are more efficient than the EWI-FP method for solving the KGD system, especially in the nonrelativistic limit regime. Finally, we studied the dynamics of the KGD system in 2D with a honeycomb lattice potential and observed some interesting phenomenons under weak/strong interaction for different ε.

References

1. Bachelot. A.: Global Existence of Large Amplitude Solutions for Dirac-Klein-Gordon Systems in Minkowski Space. Springer, Berlin, Heidelberg (1989)
2. Bao W., Cai Y.: Mathematical theory and numerical methods for Bose-Einstein condensation. Kinet. Relat. Mod., 6(1), 1-135 (2012)
3. Bao W., Cai Y.: Uniform and optimal error estimates of an exponential wave integrator sine pseudospectral method for the nonlinear Schrödinger equation with wave operator. SIAM J. Numer. Anal., 52(3), 1103-1127 (2014)
4. Bao W., Cai Y., Jia X., Tang Q.: A uniformly accurate (UA) multiscale time integrator pseudospectral method for the Dirac equation in the nonrelativistic limit regime. SIAM J. Numer. Anal., 52(5), 1-41 (2015)
5. Bao W., Cai Y., Jia X., Tang Q.: Numerical methods and comparison for the Dirac equation in the nonrelativistic limit regime. J. Sci. Comput., 71, 1094-1134 (2017)
6. Bao W., Cai Y., Jia X., Yin J.: Error estimates of numerical methods for the nonlinear Dirac equation in the nonrelativistic limit regime. Sci. China Math., 59(8), 1-34 (2016)
7. Bao W., Cai Y., Zhao X.: A uniformly accurate multiscale time integrator pseudospectral method for the Klein-Gordon equation in the nonrelativistic limit regime. SIAM J. Numer. Anal., 52(5), 2488-2511 (2014)
8. Bao W., Dong X.: Analysis and comparison of numerical methods for the Klein-Gordon equation in the nonrelativistic limit regime. Numer. Math., 120(2), 189-229 (2012)
9. Bao W., Dong X., Zhao X.: An exponential wave integrator sine pseudospectral method for the Klein-Gordon-Zakharov system. SIAM J. Sci. Comput., 35(6), A2903-A2927 (2013)
10. Bao W., Li X.: An efficient and stable numerical method for the Maxwell-Dirac system. J. Comput. Phys., 199, 663-687 (2004)
11. Bao W., Shen J.: A fourth-order time-splitting Laguerre-Hermite pseudospectral method for Bose-Einstein condensates. SIAM J. Sci. Comput., 26, 2010-2028 (2005)
12. Bao W., Zhao X.: A uniformly accurate (UA) multiscale time integrator Fourier pseudospectral method for the Klein-Gordon-Schrödinger equations in the nonrelativistic limit regime. Numer. Math., 52(5), 1-41 (2015)
13. Baumstark S., Faou E., Schratz K.: Uniformly accurate exponential-type integrators for Klein-Gordon equations with asymptotic convergence to classical splitting schemes in the nonlinear Schrödinger limit. Math. Comp., (2017) doi:10.1090/mcom/3263
14. Bjorken J. D., Drell S. D.: Relativistic Quantum Fields. Mcgraw-Hill, Inc (1965)
15. Bournaveas N.: Local existence of energy class solutions for the Dirac-Klein-Gordon equations. Commun. Part. Diff. Eq., 24, 1167-1193 (1999)
16. Bournaveas N.: Low regularity solutions of the Dirac-Klein-Gordon equations in two space dimensions. Commun. Part. Diff. Eq., 26, 1345-1366 (2001)
17. Cai Y., Yi W.: On error estimates of finite difference time domain methods for the Klein-Gordon-Dirac system in the nonrelativistic limit regime. submitted

18. Chadam M. J., Glassey R. T.: On certain global solutions of the Cauchy problem for the (classical) coupled Klein-Gordon-Dirac equations in one and three space dimensions. Arch. Ration. Mech. An., 54(3), 223-237 (1974)
19. Chen G., Zheng Y.: Solitary waves for the Klein-Gordon-Dirac model. J. Differ. Equations, 7(7), 2263-2284 (2012)
20. Ding Y., Xu T.: On the concentration of semi-classical states for a nonlinear Dirac-Klein-Gordon system. J. Differ. Equations, 256, 1264-1294 (2014)
21. Dirac P. A. M.: Principles of Quantum Mechanics. Oxford University Press, London (1958)
22. Dong X., Xu Z., Zhao X.: On time-splitting pseudospectral discretization for nonlinear Klein-Gordon equation in nonrelativistic limit regime. Commun. Comput. Phys., 16(2), 440-466 (2014)
23. Esteban M. J., Georgiev V., Séré E.: Bound-state solutions of the Maxwell-Dirac and the Klein-Gordon-Dirac systems. Lett. Math. Phys., 38(2), 217-220 (1996)
24. Fang Y. F.: A direct proof of global existence for the Dirac-Klein-Gordon equations in one space dimension. Taiwan J. Math., 8(1), 33-41 (2004)
25. Gautschi W.: Numerical integration of ordinary differential equations based on trigonometric. Numer. Math., 3, 381-397 (1961)
26. Greiner W.: Relativistic Quantum Mechanics-Wave Equations. Springer, Berlin, Heidelberg (1994)
27. Grimm V., Hochbruck M.: Error analysis of exponential integrators for oscillatory second-order differential equations. J. Phys. A: Math. Gen., 39, 5495-5507 (2006)
28. Hochbruck M., Lubich C.: A Gautschi-type method for oscillatory second-order differential equations. Numer. Math., 83, 402-426 (1999)
29. Hochbruck M., Ostermann A.: Exponential integrators. Acta Numer., 19, 209-286 (2000)
30. Holten J. W. V.: On the electrodynamics of spinning particles. Nucl. Phys. B, 356(1), 3-26 (1991)
31. Huang Z., Jin S., Markowich P. A., Sparber C., Zheng C.: A time-splitting spectral scheme for the Maxwell-Dirac system. J. Comput. Phys., 208(2), 761-789 (2005)
32. Lemou M., Méhats F., Zhao X.: Uniformly accurate numerical schemes for the nonlinear Dirac equation in the nonrelativistic limit regime. Commun. Math. Sci., 15(4), 1107-1128 (2017)
33. Lubich C.: On splitting methods for Schrödinger-Poisson and cubic nonlinear Schrödinger equations. Math. Comp., 77, 2141-2153 (2008)
34. Machihara S., Omoso T.: The explicit solutions to the nonlinear Dirac equation and Dirac-Klein-Gordon equation. Ricerche di Matematica, 56(1), 19-30 (2007)
35. Ohlsson T.: Relativistic Quantum Physics: From Advanced Quantum Mechanics to Introductory Quantum Field Theory. Cambridge University Press (2011)
36. Selberg S., Tesfahun A.: Low regularity well-posedness of the Dirac-Klein-Gordon equations in one space dimension. Commun. Contemp. Math., 10(2), 347-353 (2006)
37. Slawianowski J. J., Kovalchuk V.: Klein-Gordon-Dirac equation: Physical justification and quantization attempts. Rep. Math. Phys., 49, 249-257 (2002)
38. Strang G.: On the construction and comparision of difference schemes. SIAM J. Numer. Anal., 5, 505-517 (1968)
39. Su C.: Comparison of numerical methods for the Zakharov system in the subsonic limit regime. J. Comput. Appl. Math., 330, 441-455 (2018)
40. Yi W., Cai Y.: Optimal error estimates of finite difference time domain methods for the Klein-Gordon-Dirac system. submitted
41. Zhao X.: On error estimates of an exponential wave integrator sine pseudospectral method for the Klein-Gordon-Zakharov system. Numer. Meth. Part. D. E., 32(1), 266-291 (2016)